Title

Predicting dark respiration rates of wheat leaves from hyperspectral reflectance

Running Title

Predicting dark respiration rates of wheat leaves

Authors

Onoriode Coast[1], Shahen Shah[1,2,] Alexander Ivakov[3†], Oorbessy Gaju[1], Philippa B. Wilson[1‡], Bradley C. Posch[1], Callum J. Bryant[1], A. Clarissa A. Negrini[1], John R. Evans[3], Anthony G. Condon[3,4], Viridiana Silva-Pérez[3,4], Matthew P. Reynolds[5], Barry J. Pogson[1], A. Harvey Millar[6], Robert T. Furbank[3,4] & Owen K. Atkin[1]

Contact Information

[1]ARC Centre of Excellence in Plant Energy Biology, Research School of Biology, Australian National University, Canberra, ACT 2601, Australia; [2]The University of Agriculture Peshawar, Khyber Pakhtunkhwa 25130, Pakistan; [3]ARC Centre of Excellence for Translational Photosynthesis, Research School of Biology, Australian National University, Canberra, ACT 2601, Australia; [4]CSIRO Agriculture, PO Box 1700, Canberra, ACT 2601, Australia; [5]International Maize and Wheat Improvement Centre (CIMMYT) Int. Apdo. Postal 6–641, 06600 México, DF, Mexico; [6]ARC Centre of Excellence in Plant Energy Biology, University of Western Australia, Perth, Western Australia 6009, Australia.

Present address: [†]Australian Institute of Sport, Leverrier Street, Bruce, ACT, 2617 Australia; [‡]Grains Research and Development Corporation, Kingston, ACT 2604, Australia.

Correspondence:

Owen K. Atkin, ARC Centre of Excellence in Plant Energy Biology, Research School of Biology, Australian National University, Canberra, ACT 2601, Australia.

Email: owen.atkin@anu.edu.au

Funding

Australian Research Council (ARC) Centre of Excellence in Plant Energy Biology, Grant/Award Number: CE140100008; ARC Centre of Excellence for Translational Photosynthesis Grant/Award Number: CE1401000015; Australian Government National Collaborative Research Infrastructure Strategy (Australian Plant Phenomics Facility) – PIEPS Grant; International Wheat Yield Partnership and Grains Research Development Council Grant Number: ANU00027. Australian Government Endeavour Fellowship.

Acknowledgements

This work was supported by grants from the ARC Centre of Excellence in Plant Energy Biology (CE140100008), the ARC Centre of Excellence for Translational Photosynthesis (CE1401000015), the Australian Government National Collaborative Research Infrastructure Strategy (Australian Plant Phenomics Facility) – PIEPS grant, the International Wheat Yield Partnership and Grains Research Development Council Grant (ANU00027). We acknowledge the Endeavour Fellowship awarded to S.S. for which part of this research was developed. Two anonymous reviewers are thanked for offering suggestions that improved this manuscript.

Abstract

Greater availability of leaf dark respiration (R_{dark}) data could facilitate breeding efforts to raise crop yield and improve global carbon cycle modelling. However, the availability of R_{dark} data is limiting because it is cumbersome, time consuming or destructive to measure. We report a non-destructive and high-throughput method of estimating R_{dark} from leaf hyperspectral reflectance data that was derived from leaf R_{dark} measured by a destructive high-throughput oxygen consumption technique. We generated a large dataset of leaf R_{dark} for wheat (1380 samples) from 90 genotypes, multiple growth stages and growth conditions to generate models for R_{dark}. Leaf R_{dark} (per unit leaf area, fresh mass, dry mass or nitrogen, N) varied 7- to 15-fold among individual plants, while traits known to scale with R_{dark}, leaf N and leaf mass per area (LMA), only varied 2- to 5-fold. Our models predicted leaf R_{dark}, N and LMA with r^2 values of 0.5-0.63, 0.91 and 0.75, respectively, and relative bias of 16-18% for R_{dark} and 7-12% for N and LMA. Our results suggest that hyperspectral model prediction of wheat leaf R_{dark} is largely independent of leaf N and LMA. Potential drivers of hyperspectral signatures of R_{dark} are discussed.

Keywords:

high-throughput phenotyping, leaf reflectance, machine learning, mitochondrial respiration, proximal remote sensing, wheat (*Triticum aestivum* L.)

1 INTRODUCTION

The world's population is projected to rise by approximately 30%, reaching 9.7 billion in 2050 (United Nations Department of Economic and Social Affairs Population Division, 2015). This increase will cause demand for staple food crops to double (Cassman, 1999; Tilman, Balzer, Hill, & Befort, 2011). Doubling crop productivity to match future demand will be challenging (Tilman, Cassman, Matson, Naylor, & Polasky, 2002), a challenge exacerbated by climate change (Goldsmith, Gunjal, & Ndarishikanye, 2004; IPCC, 2013; Xiao & Ximing, 2011). Addressing these challenges will require the simultaneous pursuit of a broad range of options (Godfray et al., 2010) including increasing yield per unit of land, and identification and use of germplasm with better resilience to global climate change.

Theoretically, increasing radiation use efficiency (RUE, increase in biomass per unit absorbed radiation) provides a novel way to increase potential yield. RUE could be increased by improving photosynthesis by: (i) altering crop canopy architecture to alter the distribution of radiation capture between leaves (Loomis & Williams, 1969); (ii) introducing a carbon concentrating C_4 mechanism into C_3 plants (Furbank, von Caemmerer, Sheehy, & Edwards, 2009); and (iii) re-engineering Rubisco (Parry, Madgwick, Carvalho, & Andralojc, 2007). Another opportunity to increase RUE is to optimize mitochondrial respiration in the dark (R_{dark}). In all plants, energy from R_{dark} drives biosynthesis, cellular maintenance and active transport. The respiratory pathway also provides intermediates that serves as substrates for the synthesis of ATP, amino acids, nucleic acids, fatty acids and many secondary metabolites. The efficiency of ATP synthesis per unit of CO_2 released or O_2 consumed through the respiratory process varies, depending on engagement of phosphorylating and non-phosphorylating pathways of mitochondrial electron transport (Millar, Whelan, Soole, & Day, 2011; Vanlerberghe & McIntosh, 1997). Variations in the rate and efficiency of leaf R_{dark} thus have the potential to influence biomass accumulation and yields of crops (Hauben et al., 2009;

92 Wilson & Jones, 1982). Consequently, large datasets on leaf R_{dark} have potential application
93 in various aspects of the crop production system, including: screening of germplasm in genetic
94 resource collections and in plant breeding; assessing the efficacy of agricultural management
95 programmes; and, monitoring crop health. Of particular importance is the formation of
96 comprehensive datasets that assess genotype- and environment-mediated variation in leaf R_{dark}
97 under controlled and field conditions.

98 Leaf respiration, defined as the non-photorespiratory mitochondrial CO_2 evolution in
99 the light (R_{light}), is typically less than R_{dark} (Hurry et al. 2005; Pärnik & Keerberg, 1995).
100 Techniques for measuring R_{light}, including the Laisk (1977), Kok (1948) and/or mass
101 spectrometer (Loreto, Velikova & Di Marco, 2001) approaches, are low-throughput and often
102 challenging to correctly implement. Measuring R_{dark} is also slow and cumbersome. To address
103 the issue of low-throughput methods to measure leaf respiration, high-throughput approaches
104 have been recently developed to estimate R_{dark} by measuring O_2 consumption (O'Leary et al.
105 2017; Scafaro et al. 2017; Sew et al. 2013). Sew et al. (2013) employed a liquid-phase oxygen-
106 sensitive fluorophore technology, while Scafaro et al. (2017) and O'Leary et al. (2017) used a
107 faster, automated gas-phase method; the latter system takes only ~1-2 min per sample. Such
108 high-throughput measurements of respiratory O_2 uptake will be indicative of rates of CO_2
109 efflux in leaves where the primary respiratory substrate is sucrose and the latter is fully oxidized
110 to CO_2 and H_2O (Lambers, Chapin & Pons, 2008). However, while these approaches enable
111 rapid screening of large numbers of samples, all require destructive sampling of leaves, limiting
112 their utility for ongoing monitoring of leaf R_{dark} at the landscape scale. In the current study, we
113 outline a rapid non-destructive technique – using reflectance spectra – to estimate R_{dark}.

114 Instruments can measure electromagnetic radiation reflected from vegetation surfaces
115 spanning the visible (400-700 nm), near-infrared (NIR, 700-1300 nm), and shortwave infrared
116 (SWIR, 1400-3000 nm) spectral regions. When light falls on a leaf, it can be absorbed, reflected

or transmitted. Light absorption by leaves in the visible region is driven by electron transitions in pigments (including chlorophyll, carotenoids and anthocyanins). In the NIR-SWIR spectra region of 700-2400 nm, in contrast, light absorption is driven by the bending and stretching of covalent bonds between hydrogen atoms and atoms of carbon, oxygen and nitrogen in water and other chemicals (Curran, 1989). Radiation reflected from leaves can provide information about the internal composition of the leaf (Blackburn, 2007; Jacquemoud & Baret, 1990; Jacquemoud et al. 1996). Reflectance over a broad range of narrow and contiguous wavelength bands, termed hyperspectral reflectance, is increasingly used to predict plant or crop traits including: water status (Gutierrez, Reynolds, & Klatt, 2010; Sims & Gamon, 2003); photosynthetic metabolism (Ainsworth, Serbin, Skoneczka, & Townsend, 2014; Barnes et al., 2017; Serbin, Dillaway, Kruger, & Townsend, 2012; Silva-Pérez et al., 2018); leaf mass per area (LMA) (Asner and Martin, 2008; Asner et al., 2011; Ecarnot, Compan, & Roumet, 2013); concentrations or contents of nitrogen (N), lignin and photosynthetic pigments (Martin & Aber, 1997; Yendrek et al., 2017); and grain yield (Montesinos-López et al., 2017a, b; Weber et al., 2012).

Respiration rates at a standard temperature (25°C, R_{dark}^{25}), whether expressed on a mass or area basis, are highly variable. Variation in R_{dark}^{25} among genotypes and environments is predictable from other leaf traits such as N concentration or content, LMA and the carboxylation capacity of Rubisco at 25°C ($V_{c,max}^{25}$) (Atkin et al., 2015; Reich et al., 1998a; Reich, Walters, Tjoelker, Vanderklein, & Buschena, 1998b; Ryan, 1991). Both N and LMA can be predicted from hyperspectral reflectance data (Serbin et al., 2012; Ecarnot et al., 2013; Silva-Pérez et al., 2018). It is also possible to predict $V_{c,max}^{25}$, but with lower accuracy and precision (Ainsworth et al. 2014; Dechant, Cuntz, Vohland, Schulz, & Doktor, 2017; Doughty, Asner, & Martin, 2011; Serbin et al. 2012; Silva-Pérez et al. 2018). The poorer ability to predict $V_{c,max}^{25}$ from leaf reflectance compared to leaf N could be due to the absence of a direct

absorption signal related to $V_{c,max}^{25}$, arising instead from a secondary correlation with leaf N (Dechant et al., 2017). Both photosynthesis and respiration are processes requiring numerous proteins (Evans & Terashima, 1988; Evans, 1989a; Field & Mooney, 1986), which pose ATP demands associated with protein synthesis and repair (Hachiya, Terashima, & Noguchi, 2007) and functional linkages between photosynthetic and respiratory metabolism (Noguchi & Yoshida, 2008). Although R_{dark} scales with N, LMA and $V_{c,max,}$ and these three parameters can each be predicted with various levels of confidence from hyperspectral reflectance, we are aware of only one publication predicting R_{dark} directly from reflectance spectra (see Doughty et al., 2011). There might be limitations in prediction of a flux such as R_{dark} from reflectance spectra compared with prediction of capacity of other physiological processes e.g. $V_{c,max}$. This might be because R_{dark} is a physiological process driven by enzymatic reactions that dynamically adjust to short-term (seconds to minutes) and long-term (hours to days) environmental changes, whereas the proteins underpinning metabolic capacity can be more stable over time. In addition, respiratory enzymes may not exhibit distinct reflectance signatures that would enable direct quantification as such. Estimation of leaf R_{dark} may arise indirectly through secondary correlations with other leaf traits e.g. leaf N and LMA, as already discussed for $V_{c,max}^{25}$ (Dechant et al., 2017). Here, we investigate the possibility that variations in R_{dark} can be well predicted from hyperspectral signatures.

Appropriate analytical tools for assessing plant traits using hyperspectral reflectance data includes Partial Least Square Regression (PLSR, Wold, Sjöström, & Eriksson (2001)), which combines features from principal component analysis and multiple regression, and machine learning algorithms such as Support Vector Machine Regression (SVMR, Vapnik (1995)). One of the most commonly used analytical tool in estimating plant traits from hyperspectral reflectance of leaves is PLSR. Doughty et al. (2011) used PLSR to predict R_{dark} from leaf hyperspectral reflectance collected from 149 species ~~(see Doughty et al., 2011).~~

~~However, prediction of R_{dark} in that study was limited~~(r^2=0.48, RMSE=-0.52 µmol m^{-2} s^{-1}; and for canopy R_{dark} r^2=0.16, RMSE=0.58 µmol m^{-2} s^{-1}). This encouraged us to see if the method could be applied to wheat leaves.

To test the suitability of estimating leaf R_{dark} from hyperspectral reflectance data, three experiments were conducted during which we characterised leaf R_{dark}, hyperspectral reflectance, biochemical (N concentration) and morphological (LMA) traits under different environmental conditions, and plant growth stages, using a diverse set of wheat (*Triticum aestivum* L.) genotypes. We report on leaf respiration rates and associated leaf traits of 1380 samples from 90 genotypes. The varied conditions, growth stages and genotypes were used to generate a wide range of R_{dark} values to robustly test different modelling approaches. We used two independent analytical tools –PLSR and SVMR to investigate if:

1. Leaf R_{dark} can be well predicted from leaf hyperspectral reflectance data
2. Model predictions of leaf R_{dark} from spectral reflectance data can be improved by using an alternative to PLSR, i.e. SVMR

Our study also provided an opportunity to assess the extent of genotypic and environment-driven variation in leaf respiration rates of commercial elite wheat lines, and the extent to which other traits such as leaf N and LMA are predictors of wheat leaf R_{dark} values.

2 MATERIALS AND METHODS

Three independent experiments were conducted to explore associations (or the absence thereof) between leaf reflectance spectra and leaf R_{dark} in wheat. Two of the experiments (Experiments 1 and 2) were undertaken in climate-controlled glasshouses at the Australian National University (ANU), Canberra while a third (Experiment 3) was conducted in a field-based poly-tunnel at CSIRO Ginninderra Experiment Station. Leaves of a diverse set of wheat genotypes

(between 3 and 70 per experiment, see Table S1 for list of genotypes) were examined at different growth stages and under varied environmental conditions (Table 1). The varied growth stages and environmental conditions were used to generate a wide range of R_{dark} values and to ensure a robust test of our approach of using leaf reflectance spectra to predict leaf R_{dark}.

2.1 Glasshouse Experiment 1 – exploring environment-induced variation in leaf respiration

Experiment 1 was carried out at the ANU Controlled Environment Facilities, Canberra, Australia. Three wheat genotypes, 'Calingiri', 'Halberd', and 'Janz', were selected to represent a wide range of average rates of R_{dark}; an earlier study screening 138 lines (grown in controlled environment cabinets) showed two-fold genotypic variation in R_{dark} among the wheat lines, with 'Calingiri', 'Halberd', and 'Janz' being at high (0.79 µmol O_2 m^{-2} s^{-1}), mid (0.50 µmol O_2 m^{-2} s^{-1}) and low (0.35 µmol O_2 m^{-2} s^{-1}) range of R_{dark} values, respectively (Scafaro et al., 2017). Seeds were germinated on moist filter papers on 09 March 2016 with >95% germination achieved within two days. Five days after germination (DAG; on 16 March 2016) seeds were transferred into 2 L plastic pots (one seedling per pot) filled with Martins mix (Martins Fertilizers Ltd, Yass, NSW Australia). The potting mix was treated at 63°C for 1 h prior to filling pots. The mix was enriched with Osmocote® OSEX34 EXACT slow-release fertilizer (Scotts Australia, Bella Vista, NSW, Australia). The base of the plastic pots were perforated in several places to ensure proper drainage upon watering. Seedlings were watered twice daily, in the morning and late afternoon, to avoid water deficit stress. The glasshouse was maintained at 12/12 h day/night temperature of 28/23°C and ambient light condition. One-week old seedlings were transferred to different treatments as per the experimental design described below.

The experimental design was a split-split-plot with temperature, light and genotype, respectively as main, sub and sub-sub plots, replicated six times. There were three growth

temperatures (12/12 h day/night conditions of 21/16, 28/23 and 35/30°C), two light intensities [photosynthetic photon flux density (PPFD) of 600~800 µmol m^{-2} s^{-1} (high light) and 150~200 µmol m^{-2} s^{-1} (low light, i.e. 25% of high light)] and three genotypes ('Calingiri', 'Halberd', and 'Janz'). The temperature regimes were maintained by automated heating and cooling systems. Changes in temperature occurred at 0700/1900 h. The prevailing ambient light was taken as high light and to achieve low light a green mesh was placed over bespoke-cages within which plants were kept (see Figure S1). This mesh and cage arrangement resulted in a 75% reduction of ambient light reaching the plants. Photoperiod during that time of the year was ~12 h day^{-1}. Plants were kept under these conditions for three weeks, at the end of which plants were approximately at growth stage Z13 (seedling growth; Zadoks, Chang, & Konzak, 1974). The most recently expanded leaf (the third true leaf and henceforth designated as Leaf-3) was measured at 35 and 36 DAG; the first three replicates at 35 DAG and the rest at 36 DAG. We used 108 plants/leaf samples for Experiment 1.

2.2 Glasshouse Experiment 2 – variation in leaf respiration among 70 genotypes

Experiment 2 was conducted in the same glasshouse facility as Experiment 1. Seeds of seventy wheat genotypes (see Table S1 for list of genotypes), a subset of the 138 genotypes used recently to validate a technique for high-throughput measurement of R_{dark} (Scafaro et al., 2017). The seeds were germinated and transferred into 2 L plastic pots filled with Martins mix as in Experiment 1. Seedlings were transferred on 09 June 2016 (6 DAG). Plant nutrition and watering were as described for Experiment 1. The glasshouse was maintained for three consecutive months at 12/12 h day/night temperature of 25/20˚C with temperature changes at 0700/1900 h. Light measured as PPFD at plant height varied between 400 and 1200 µmol m^{-2} s^{-1} and photoperiod during this experiment was 10-12 h day^{-1}.

The experimental design was a randomised complete block design with four replicates. Due to space limitations, the four replicates were split equally between two adjoining rooms in a glasshouse. Each replicate, consisting of 70 genotypes, was placed on a bench in a glasshouse (n=280 plants). Each glasshouse room had a pair of benches. Leaf measurements were taken first at growth stage Z13 (seedling growth; 24-27 DAG) from Leaf-3, and then at growth stages Z61-69 (anthesis) from the leaf subtending the flag leaf (henceforth designated as Flag-1; 67-70 DAG) and the flag leaf (81-85 DAG) and. For each growth stage, measurements and sample collection were completed within 4-5 days. Each of the four replicates required at least one day for data collection. Total leaf samples used for Experiment 2 were 840.

2.3 Poly-tunnel Experiment 3 – variation in leaf respiration among 24 wheat genotypes

Seeds of 24 wheat genotypes (selected based on similarities in phenology - height and days to anthesis, but contrasting for $V_{c,max}$ and R_{dark}) were used for this experiment. Seeds were sown at a rate of 250 grains m^{-2} on 16 September 2016 in field plots, under a poly-tunnel, at CSIRO Ginninderra Experiment Station, Australian Capital Territory (35° 12´S, 149° 06´E; 600 m asl). The soil was a yellow chromosol (Isbell, 2002). Mean daily maximum/minimum air temperature obtained from a weather station installed in a neighbouring poly-tunnel from November to December was 27/12°C. A 30-year (1981-2010) average over the same period was 25/11°C, and from September through December was 22/8°C (data from the closest Bureau of Meteorology weather station). The photoperiod during the experiment was 12-14 h day^{-1}. Plants were kept well-watered by drip irrigation and fertilized optimally. The experiment was laid out as a row × column design with 12 rows and six columns, with each block containing two columns. As such, there were 72 plots, each block of 24 genotypes replicated three times. Each plot consisted of ten equally spaced 1m rows covering an area of 2.5 m^2.

Measurements and sampling were at growth stages Z23-27 (tillering) and Z55-71 (inflorescence emergence, anthesis through milk development). At both growth stages three sampling events were carried out on consecutive days. At growth stages Z23-27 (tillering), sampling and measurements were on the last fully expanded leaf, with one leaf measured from each plot each day for three days. The leaf sampled varied between Leaf-3 and the sixth true leaf 6 (Leaf-6), when counting from the base of the plant. At growth stages Z55-71 (inflorescence emergence, anthesis through milk development), the flag leaf and Flag-1 were sampled on the first and second day, respectively, while on the third day the leaf subtending Flag-1 (designated as Flag-2) was sampled. In total, 432 leaf samples were collected for Experiment 3.

2.4 Measured traits – all experiments

Reflectance spectra were captured from the adaxial surface of leaves using an ASD FieldSpec® 4 Full-Range spectroradiometer (Analytical Spectral Devices, Inc., Boulder, CO, USA) with spectral range 350-2500 nm and a rapid data collection time of 0.1s per spectrum. Data from the full spectral range (350-2500 nm) was used for analysis. Spectral resolution of the device was 3, 10 and 10 nm (Full-Width-Half-Maximum) at 700, 1400 and 2100 nm, respectively. Sampling intervals were 1.4 and 2 nm for the spectral regions 350-1000 nm and 1000-2500 nm, respectively. The device was fitted with an ASD fibre optic cable and leaf clip. A mask attached to the leaf clip reduced the width of the aperture through which leaf reflectance was recorded to 11.5 mm, enabling easier measurement of leaf widths down to 12 mm (Silva-Pérez et al., 2018). Leaf spectral reflectance was captured between 1000 and 1400 h from the adaxial surface and close to the midpoint of the leaf. Each leaf was measured at one position, taking less than 20s. An internal light source was used to illuminate a white reference panel for calibration or a leaf placed in front of a black panel during measurement. After measuring the reflectance spectrum, the leaf was immediately detached near the ligule for subsequent

286 measurement of R_{dark}. Samples were temporarily stored in ziplock bags with moist tissue paper
287 or cotton balls and placed in Styrofoam boxes partly filled with ice blocks/packs for transfer
288 from glasshouse/field to the laboratory. R_{dark} values were determined within 24 h of obtaining
289 spectral reflectance values. Leaf sections of ~4 cm^2, including the exact spot where the
290 reflectance measurement was taken from, was dissected from the whole leaf and used for
291 determination of other traits.

292 The dissected leaf section was weighed and exact area determined. The ~4 cm^2 leaf
293 sections were placed in an automated Q2 O_2-sensor (Astec Global, Maarssen, the Netherlands)
294 to determine O_2 consumption rate following the method of Scafaro et al. (2017). Briefly, freshly
295 dissected leaf tissues were placed in 2 mL tubes and hermetically sealed with specialised caps
296 (Astec Global). The top surfaces of caps contained a fluorescent metal organic dye, sensitive
297 to O_2 quenching. The tubes were loaded onto racks, which individually accommodated 48
298 tubes, and racks placed on the Q2 O_2-sensor. Each rack was loaded with two tubes filled with
299 ambient air (designated 100% O_2) and N_2 (designated as 0% O_2), for calibration of the Q2 O_2-
300 sensor before measurement was made. An automated robotic arm with fibre optic fluorescence
301 detection capability scanned the rows of tubes enabling the quantification of O_2 dependent
302 decay in fluorescence signal. The % O_2 relative to the air calibration tube was converted to
303 absolute values of R_{dark} in moles of O_2 s^{-1}. The Q2 O_2-sensor was set at 25°C and measurements
304 taken at a frequency of four minutes over a two-hour period. However, values from the first 30
305 min were disregarded, as they tend to be unstable – respiratory activity rapidly increased and
306 decreased during this period (Scafaro et al., 2017).

307 All leaf samples used for determination of R_{dark} were oven-dried at 70°C for 48 h
308 (Experiment 1 and 2) or 60°C for 72 h (Experiment 3) then LMA determined. The same
309 samples were then used to determine leaf N content (%), by combustion using a Carlo-Erba
310 elemental analyser (NA1500, Thermo Fisher Scientific, Milan, Italy). Area, fresh mass, dry

mass and N content (per gram of leaf dry mass, N_{mass}, or per square metre of leaf area, N_{area}) of the leaf section used for determination of R_{dark} were used to calculate R_{dark} per: (i) square metre of leaf area (R_{dark_LA}, μmol O_2 m_{LA}^{-2} s^{-1}); (ii) gram of leaf fresh mass (R_{dark_FM}, nmol O_2 g_{FM}^{-1} s^{-1}); (iii) gram of leaf dry mass (R_{dark_DM}, nmol O_2 g_{DM}^{-1} s^{-1}); and (iv) gram of leaf N_{mass} (R_{dark_N}, nmol O_2 gN^{-1} s^{-1}).

2.5 Model development for prediction of leaf traits from reflectance spectra

Different regression techniques, including PLSR and SVMR have been used to quantify relationships between spectra data and leaf/canopy traits. But only PLSR has been used to predict leaf/canopy R_{dark} of 149 species (for prediction of leaf R_{dark} r^2=0.48, RMSE=-0.52 μmol m^{-2} s^{-1}; and for canopy R_{dark} r^2=0.16, RMSE=0.58 μmol m^{-2} s^{-1}; Doughty et al., 2011), although not including wheat. The SVMR is considered a powerful regression technique (Thissen, Pepers, Üstün, Melssen, & Buydens, 2004), in terms of model performance and prediction accuracy. Therefore, we independently tested the different models for leaf traits using these two regression techniques.

Prior to data analysis a multiplicative correction module (ASD Spectral Analysis and Management System (SAMS®) version 3.2) was applied to the reflectance data at 1000 and 1800 nm to correct for 'jumps' observed in apparent reflectance at the intersections between different detector ranges. As did Silva-Pérez et al. (2018), reflectance spectra with values greater than 0.7 between 800 and 1000 nm were treated as an outlier and removed.

Variation in foliar traits (including R_{dark}) and biochemical composition based on leaf optical properties were modelled using PLSR and SVMR. The PLSR technique could be performed with either the continuous, full-spectrum data (Asner & Martin, 2008) or a pre-determined spectral subset (Bolster, Martin, & Aber, 1996). We initially applied the PLSR model building approach of Serbin et al. (2012) and Wold et al. (2001) to 90% of the dataset

(training dataset). This works by extracting latent variables (i.e. underlying factors or indices produced by the observable variables that account for most of the variation in the response) from sampled factors and responses. This step is analogous but not identical to principal component regression. Then the extracted factors are applied in a set of regression equations and used to construct predictions of the responses. PLSR models can suffer from over-fitting if the number of model components selected is suboptimal. To avoid overfitting, we selected the optimal number of model components for the PLSR model by minimizing the root mean squared error of prediction. The root mean squared error of prediction was calculated by k-fold cross validation. The optimal PLSR model was subsequently applied to estimate measured traits of the remaining 10% of dataset (test dataset). This was done independently for each trait of interest.

Like our PLSR model, we initially built the SVMR model on 90% of the dataset (training dataset) then subsequently used the built model to estimate measured traits of the remaining 10% (test dataset). To develop our SVMR models we used the epsilon-regression form of SVMR and followed the recommendation of Hsu, Chang, & Lin (2003). We chose the Gaussian (radial basis function) kernel type for our model. The radial basis function is a general purpose kernel used when there is no prior knowledge about the data. Then we combined this with a k-fold (k=10) cross validation approach that optimized for model cost parameter (C) and kernel parameter (γ). Cost and kernel parameters resulting in the best model fit, i.e. highest squared Pearson correlation (r^2) on the training dataset, were selected. This was then used to calculate validation statistics for the test dataset (the remaining 10% of dataset not used for model building).

PLSR and SVMR analyses were carried out in the R statistical environment (R Core Team, 2018) using the packages ‘pls’ (Mevik, Wehrens, & Liland, 2016) and ‘e1071’ (Meyer, Dimitriadou, Hornik, Weingessel, & Leisch, 2017), respectively. Model predictions for 90/10

training/test datasets were compared for PLSR and SVMR and for all three experiments combined based on their r^2, RMSE and relative bias (%). In addition, we undertook model validation by predicting R_{dark} of individual or combined experiments using hyperspectral-based models built on individual experiments or various combinations of experiments.

2.6 Statistical analysis

Leaf R_{dark}, N and LMA were subjected to ANOVA after tests for normality (Bartlett's test and visual assessment of Q-Q plot) and homogeneity of variances (Shapiro-Wilk's test and plots of residuals against fitted values). Outliers were identified and removed from the dataset using the Tukey's method i.e. values above and below the 1.5*IQR (the inter-quartile range) were removed. Tukey's method was chosen over the standard deviation method because it is independent of the distribution of the data and is resistant to extreme values.

3 RESULTS

3.1 Leaf reflectance spectral properties

Leaf reflectance spectra varied substantially within and between experiments (Figure 1 and Figure S2). For example, reflectance at 400 nm ranged between 0.04-0.07 (Experiment 1), 0.03-0.11 (Experiment 2) and 0.03-0.17 (Experiment 3, Figure S2). Across all experiments, the largest range in leaf reflectance was in the NIR region. However, the coefficient of variation (CV) of reflectance for this region was the least (23%) compared to 33% for the SWIR and 32% for the visible regions. The wavelengths with the largest and smallest range of reflectance were 1926 nm (79%) and 1076 nm (21%), respectively.

3.2 Variation in leaf traits

Leaf R_{dark_LA}, R_{dark_FM} and R_{dark_DM} across experiments were on average 0.73 μmol O_2 m_{LA}^{-2} s^{-1}, 4.05 nmol O_2 g_{FM}^{-1} s^{-1}, and 21.1 nmol O_2 g_{DM}^{-1} s^{-1}, respectively, showing a seven- to nine-fold variation (Table 2). Leaf R_{dark_N} averaged 449 nmol O_2 g_N^{-1} s^{-1} spanning a 15-fold range of values (87-1260 nmol O_2 g_N^{-1} s^{-1}). The large range in R_{dark_N} compared to other traits was also characterised by ~25% higher CV than R_{dark_LA}, R_{dark_FM} or R_{dark_DM} (CV=0.37 for R_{dark_N} vs 0.28-0.29 for others; Table 2). Leaf N_{mass} averaged 49.5 mg g^{-1} (CV=0.28), N_{area} 0.87 g m^{-2} (CV=0.21) and LMA 31.5 g m^{-2} (CV=0.29) with two- to and five-fold variation (Table 2). Table 2 provides a summary of leaf traits for each and all experiments combined. Treatment or leaf level summaries and ANOVA results for experiments 1, 2 and 3 are provided in Tables S2, S3 and S4, respectively. Broadly, rates of R_{dark} were affected by growth irradiance, with markedly lower rates in plants grown under low light compared to those under high light, with inconsistent effects of growth temperature R_{dark} (measured at 25°C) (Table S2). Growth stage was also found to have strong effects on R_{dark}, albeit with the differences between vegetative and reproductive varying depending on the units that R_{dark} was expressed (Tables S3 and S4).

3.3 Correlations of leaf respiration with other leaf traits

Correlations of R_{dark} with leaf N and LMA were poor (r between -0.08 and 0.38), irrespective of the units that rates were expressed in (Figure 2 and Table 3), with the exception between R_{dark_N} and leaf N_{mass} (r=-0.59). See Figure S3 for more detailed results of individual experiments. The signs of the correlations of R_{dark} with leaf N_{mass} and LMA differed, with R_{dark} having a negative association with leaf N_{mass}, except for R_{dark_DM}, whereas R_{dark} had a positive association with LMA, except for R_{dark_DM}. Leaf N_{mass}, N_{area} and LMA correlated significantly (P<0.001) with one another albeit poorly (r=0.12-0.49; Figure 3, Table 3. Also see Figure S4 for individual experiments).

3.4 Predictions of leaf respiration and other traits based on a subset of pooled experimental data (10% test dataset)

We validated our models using a test dataset that consisted of 10% of our pooled experimental data, which was not used in building the models. Across experiments, predictions of leaf R_{dark} varied per unit leaf area, DM and N (r^2=0.50-0.63 for PLSR, Figure 4 and r^2=0.53-0.64 for SVMR, Table 4). Values of r^2 were generally highest for R_{dark} per leaf N and least when expressed per gram of leaf dry mass (Table 4). Relative bias were between 16 and 18% (Table 4). Model predictions of leaf N_{mass}, N_{area} and LMA achieved r^2 of 0.91, 0.60 and 0.75, respectively with PLSR (Figure 5). For SVMR, predictions of N_{mass}, N_{area} and LMA had r^2 of 0.90, 0.79 and 0.72, respectively. The corresponding relative bias were 7-12% for PLSR, and 8-11% for SVMR.

3.5 Comparison of PLSR and models

Performance of the PLSR model was comparable to that using SVMR, with similar r^2 and RMSE, and differences in relative bias under 2% (Table 4). A similar result (i.e. no clear indication that SVMR outperformed PLSR) was obtained using a multi-method ensemble developed by Feilhauer, Asner, & Martin (2015) and tested on either the continuous, full spectrum data or a spectral subset that were selected based on weightings (Table S5; Also see Supplementary Text S1 for our attempt to reduce model complexity and improve prediction using the multi-method ensemble of Feilhauer et al. (2015)). The presentation of further results will therefore be limited to those from PLSR models using the full spectral range.

3.6 Cross-predictions of leaf respiration and other traits of experimental data

PLSR models built on one experiment were poor at predicting R_{dark} of a different experiment (Figs 6 and S5). The best outcome was predicting R_{dark_LA} for Experiment 1 using a model developed from Experiment 2 (r^2=0.33). Similarly, models built on single glasshouse

experiments were poor at predicting that of the field experiment and vice versa. The best r^2 for this method was 0.21, for a model built from Experiment 3 predicting R_{dark_DM} for glasshouse Experiment 2. By contrast, predictions of R_{dark} based on models built on a combination of Experiments 1 and 2 or all three experiments, were better than or similar to models built on one experiment (Figs 6 and S5). For example, a model developed on 90% of data comprising all three experiments predicted (i.e. was validated on) R_{dark_DM} of the remaining 10% of data for each of Experiment 1, 2 and 3 with r^2 of 0.20, 0.66 and 0.61 respectively. This compares to r^2 of 0.04, 0.61 and 0.45 when models were built with 90% of data solely from same experiment and validated on the remaining 10%. Similar results were obtained with N_{area} (Figs 7 and S6).

4 DISCUSSION

Our study has produced a large dataset of wheat leaf R_{dark} rates (1380 samples), obtained from 90 genotypes, multiple growth stages and grown under varying environmental conditions. We show that leaf R_{dark} can be predicted from reflectance spectra with model r^2 values of 0.50-0.64 and relative bias of 16-18%. PLSR model predictions of leaf R_{dark} from spectral reflectance data were as good as SVMR. Models predicting R_{dark} from leaf reflectance spectra generally performed better when trained on more diverse data, such as genotype, growth stage and growing conditions. Our ability to predict R_{dark} from reflectance spectra could arise from: (i) indirect association with other traits (e.g. N_{area}, N_{mass} and LMA); (ii) links with spectral signatures of key photosynthetic components such as V_{cmax} and/or J_{max} whose variations are coupled with variations in R_{dark}; and (iii) spectral absorption features by respiratory substrates or components in the respiratory system. These possibilities are discussed in detail in section 4.2.

4.1 Variation in wheat leaf respiration and other leaf traits.

Wheat leaf R_{dark} varied enormously, irrespective of how it was expressed. The seven-fold variation in wheat leaf R_{dark_LA} reported here is higher than the modest two-fold reported by Scafaro et al. (2017) for wheat and by O'Leary et al. (2017) for Arabidopsis (*Arabidopsis thaliana* L.). It is comparable to the 10-fold variation for 899 species covering plant functional types from the Arctic to the tropics (Atkin et al., 2015). Variations reported here for wheat leaf N and LMA were in line with other reports for wheat (Ecarnot et al., 2013; Martin et al., 2018), other crops (Jullien, Allirand, Mathieu, Andrieu, & Ney, 2009) and within natural ecosystems (Asner et al., 2014; Wright et al., 2004). These variations were caused by genotypic, growth and environmental effects. For instance, the plot of leaf R_{dark_DM} versus N_{area} (Figure 2c) showed distinct clusters of the vegetative and reproductive stages of both Experiments 2 and 3. Also, the plot of R_{dark_LA} versus N_{area} (Figure 2a) could be distinguished by Experiment, with higher R_{dark_LA} per leaf N_{area} for Experiment 2 compared to Experiment 3. The higher leaf R_{dark} per leaf N_{area} during growth stages Z13/Z23-27 (i.e. seedling growth/tillering) of Experiments 2 and 3 or of some genotypes compared to others suggests greater relative allocation of leaf N to metabolic processes than to structural properties (Evans, 1989a, b; Harrison, Edwards, Farquhar, Nicotra, & Evans, 2009), higher demand for respiratory products and/or increase in ATP turnover (Atkin & Tjoelker, 2003; O'Leary et al., 2017).

In natural ecosystems and even within species, individual plants experiencing cold growth conditions can exhibit higher temperature-normalized rates of leaf R_{dark} than individuals of the same genotypes growing in warmer habitats (Atkin, Scheurwater, & Pons, 2006; Mooney, 1963; Oleksyn et al., 1998; Xiang, Reich, Sun, & Atkin, 2013). Cooler growth temperatures can induce increases in density and ultrastructure of mitochondria (Armstrong, Logan, & Atkin, 2006a; Armstrong, Logan, O'Toole, Tobin, & Atkin, 2006b; Miroslavov & Kravkina, 1991) and increase capacity of individual mitochondria (Armstrong et al., 2006b) both potentially contributing to the variation in leaf R_{dark}. However, variations in leaf R_{dark} and

other leaf traits reported in this study were likely in response to a combination of factors, in addition to temperature. Other factors such as growth irradiance and evaporative demand that differed among the experiments and play key roles in moderating leaf R_{dark}, N and LMA (Lusk, Reich, Montgomery, Ackerly, & Cavender-Bares, 2008; Poorter, Niinemets, Poorter, Wright, & Villar, 2009) may also have contributed.

4.2 What underpins the ability to predict leaf respiration from leaf reflectance?

Hyperspectral reflectance characteristics of leaves have been used to predict LMA, leaf N and photosynthetic traits. Extending this approach to predict R_{dark} seemed plausible given that R_{dark} scales with LMA (Wright et al., 2006), leaf N (Reich et al., 1998a, 2008; Ryan, 1991; Wright et al., 2004) and photosynthesis (Bouma, De Visser, Van Leeuwen, De Kock, & Lambers, 1995; O'Leary et al., 2017). While the prediction of R_{dark} could in part be related to N or LMA, in our study, clear and simple correlations were not evident (Figure 2a, b). Predicting R_{dark} using multiple linear regression against N and LMA only achieved r^2 values up to 0.12 (supplementary Table S6) compared to 0.54 achieved with PLSR. Allocation of leaf N to respiratory proteins, respiratory energy needed for protein turnover, and utilization of N in building thicker and denser leaves all link R_{dark} to N and LMA. The weak relationship between R_{dark}-N-LMA when R_{dark} and N are expressed on an area basis is not uncommon (Hirose & Werger, 1987; Reich, Walters, & Ellsworth., 1997, 1998a; Wright et al., 2004). Similar weak relationships have sometimes been observed between CO_2 assimilation rate and N_{area} (Reich & Walters, 1994). We also found weak relationships between R_{dark}-N and R_{dark}-LMA on a mass basis, which contrasts with the general literature dominated by interspecific studies (Reich et al., 1998a; Wright et al., 2004). However, reported relationships for intraspecific studies have been mixed (Byrd, Sage, & Brown, 1992; Fan et al., 2017; Hirose & Werger, 1987). This indicates a weak coupling of N, protein content and leaf structure to leaf R_{dark} within species such as wheat, which may be due to a range of factors, including the extent

503 to which the genotypes differed in the degree of adenylate restriction (i.e. ADP concentrations
504 and ADP/ATP ratios) of mitochondrial electron transport (Hoefnagel & Wiskich, 1998).

505 Photosynthesis and R_{dark} are interrelated. The substrates for R_{dark} required to power
506 processes such as protein turnover and phloem loading are provided by photosynthesis. Our
507 ability to predict R_{dark} might be an indirect reflection of photosynthesis. Considering that the
508 light saturated ambient rate of photosynthesis and the two major determinants of photosynthetic
509 performance – $V_{c,max}$ and J_{max} – can also be predicted from leaf reflectance (Ainsworth et al.,
510 2014; Barnes et al., 2017; Dechant et al., 2017; Doughty et al., 2011; Heckmann, Schlüter, &
511 Weber, 2017; Serbin et al., 2012 Silva-Pérez et al., 2018; Yendrek et al., 2017), one possibility
512 is that variations in R_{dark} are coupled to variations in $V_{c,max}$ and/or J_{max}, and that the ability to
513 predict R_{dark} from leaf reflectance is, in part, due to spectral signatures of key photosynthetic
514 components. Dechant et al. (2017) reported that the prediction of $V_{c,max}^{25}$ from leaf reflectance
515 is a secondary one, driven primarily by the prediction of leaf N. However, since the prediction
516 of R_{dark} here for wheat using N_{area}, LMA or their combination was poor (for R_{dark}-LA, highest
517 r^2=0.12) compared to the PLSR model (See Table S6 for multiple regression results for R_{dark}-
518 LA), our success in predicting R_{dark} indicates that there is additional information contained
519 within the reflectance spectra associated with R_{dark}.

520 Spectral signatures associated with R_{dark} could be related to respiratory substrates or
521 components in the respiratory system. These could include: (i) the abundance of sugars, organic
522 acids and adenylates (ATP and ADP); (ii) abundance of respiratory enzymes with distinct
523 spectral properties; or (iii) aspects of mitochondrial mass or lipid composition. Both leaf starch
524 and sugar content are correlated with R_{dark} (Noguchi, 2005; O'Leary et al., 2017; Peraudeau et
525 al., 2015) and they have both been estimated from hyperspectral reflectance within the range
526 reported in this study (Curran, 1989; Ramirez et al., 2015). Cytochrome *c* oxidase (COX) a
527 respiratory protein complex) in the mitochondrial respiratory chain also exhibit spectral

528 characteristics (Appaix et al., 2000; Mason, Nicholls, & Cooper, 2014;). Connections between
529 O_2 consumption, COX and spectra absorbance in vegetables have been shown (Makino,
530 Ichimura, Kawagoe & Oshita, 2007; Makino, Ichimura, Oshita, Kawagoe & Yamanaka, 2010),
531 but Umbach, Lacey & Richter (2009) argued against a direct functional link between AOX and
532 floral reflectance, which probably also applies to leaf O_2 consumption, AOX and reflectance.
533 Another possibility is that the recent discovery of an association between mitochondrial
534 functions and cell wall properties in plants (Hu et al., 2016) may indirectly link surface
535 reflectance with respiratory processes. The reliability of our model prediction of R_{dark} (r^2 0.50-
536 0.64) was considerably less than that for N (r^2=0.91), which probably represents the fact that
537 R_{dark} is determined by a complex and varied array of components. Clearly, further research is
538 required to understand the mechanistic basis underpinning leaf R_{dark} estimation from spectral
539 reflectance signatures, possibly by using mutants, sampling at different times of the day, or
540 treatments which alter photosynthetic capacity, levels of respiratory substrates and
541 mitochondrial proteins.

542 **4.3 Model cross prediction improved with data from other experiments**

543 Our models, whether built on the whole spectrum (350-2500 nm) or a selected subset of
544 wavelengths, gave good predictions of R_{dark} and other leaf traits for subsets of data not used to
545 build the models. However, predictions of leaf traits for one experiment based on models built
546 on a different experiment were poor (Fig 6, 7, S5 and S6). Poor model performance across
547 experiments is not uncommon. Silva-Pérez et al. (2018) reported that models derived from
548 field-grown aspen leaves (*Populus tremuloides* Michx.) (Serbin et al., 2012), gave poor
549 predictions when applied to wheat leaves. The predictive performance of multivariate
550 regression models may be increased by training models with more diverse data. For example,
551 r^2 for Experiment 3 R_{dark_LA} PLSR model, which was trained on just Experiment 3 data were
552 significantly lower than predictions of the same data using a model trained with data from all

three experiments (Fig 6). Development of a system for adding novel data to an existing large spectral library for retraining models could prove to be a large cost-saving measure for large scale breeding trials and ecosystem management projects. This approach, called spiking, has been successfully applied in other fields such as soil biochemistry (Guerrero et al., 2014, 2016; Guerrero, Zornoza, Gómez, & Mataix-Beneyto, 2010). Further research is needed, however, to determine the minimum data from a novel source required to achieve good model predictions of traits.

4.4 Machine learning approaches to improve model performance

To test if model prediction of R_{dark} could be improved by using alternatives to PLSR, we applied SVMR and compared the results with those from PLSR. Our comparison suggests model prediction was not limited by the use of PLSR. In addition, an independent comparison of PLSR with SVMR and Random Forest Regression (RFR, Breiman (2001)) using a different modelling approach reported by Feilhauer et al. (2015), namely a multi-method ensemble, which included PLSR, SVMR and RFR, still showed PLSR was as good as the alternatives (Table S5; Text S1). Heckmann et al. (2017) carried out a similar comparison of model performance across a wider range of algorithms for predicting crop trait from leaf reflectance and preferred PLSR models because it yielded the highest predictive power.

The ensemble of Feilhauer et al. (2015), which used a multiplicative aggregation of variable importance values of three models (PLSR, SVMR and RFR) for identification and selection of spectra bands of importance, led to the selection of 173-271 wavelengths. Model building using the selected wavelengths resulted in further improvements in model fits and prediction accuracy. Serbin et al. (2012), using a different method combined with PLSR, also reported consistently good model prediction and accuracy with fewer wavelengths. This indicated that a large fraction of the wavelengths did not provide predictive power in estimating

577 $R_{dark,}$ which is not surprising given that leaf reflectance spectra are highly collinear, as can be
578 seen from both observations and leaf radiative transfer models such as PROSPECT
579 (Jacquemond & Baret, 1990). Focusing on specific wavelengths has numerous implications for
580 downstream practise, including in scaling from leaf to vegetation canopy scale and in designing
581 simpler sensors at key wavelengths (Serbin et al., 2012).

582 **4.5 Prediction of R_{dark} based on O_2 consumption or CO_2 evolution**

583 During leaf respiration, the flux of O_2 consumption relative to CO_2 evolution, depends on the
584 substrate being metabolised (1 for carbohydrate, >1 for lipids). Importantly, 20-80% of daily
585 fixed carbon is released back into the atmosphere by whole-plant R_{dark} (Poorter, Remkes, &
586 Lambers, 1990), with leaves accounting for ~50% of whole-plant R_{dark} (Atkin, Scheurwater, &
587 Pons, 2007). It is possible to measure R_{light} or R_{dark} as CO_2 evolution in an open, flow through
588 gas exchange system using an infra-red gas analyser. Alternatively, if one wishes to measure
589 O_2 consumption, it is necessary to use a closed system to enable a sufficiently large change in
590 O_2 concentration to be detected. The large difference in concentration between CO_2 and O_2 in
591 air generally preclude simultaneous measurements of both without specialised instrumentation
592 (Beckmann, Messinger, Badger, Wydrzynski & Hillier, 2009). We chose to measure R_{dark} from
593 O_2 consumption as the rapid measurements allowed more material to be sampled (O'Leary et
594 al., 2017; Scafaro et al., 2017). Although we only validated with data on R_{dark} derived from O_2
595 consumption, our high-throughput approach can be adapted to measures of R_{dark} derived from
596 CO_2 evolution in cases where sucrose is the predominant respiratory substrate and the
597 respiratory quotient is unity (Lambers et al. 2008).

598 **4.6 Conclusions**

599 Using a diverse set of wheat genotypes measured at different growth stages and grown under
600 varied environmental conditions (light and temperature) either in glasshouses or field settings),

601 we have created a large wheat leaf R_{dark} dataset and found that R_{dark} varied enormously. R_{dark}
602 can be predicted from leaf reflectance spectra, with r^2 as high as 0.63 (when expressed per
603 gram of N with RMSE=102.4 nmol O_2 g_N^{-1} s^{-1} and relative bias=18.2%). The performance of
604 models built to predict R_{dark} were similar for both PLSR and SVMR approaches. Predictions
605 were not tightly linked to the relationships between leaf R_{dark} and LMA or leaf N. This finding
606 highlights the potential for rapid, non-invasive monitoring of various aspects of leaf energy
607 metabolism in wheat. Such advances will provide opportunities for large scale field
608 experiments to identify variants in wheat R_{dark} specifically, and wheat energy use efficiency
609 more broadly.

ACKNOWLEDGEMENTS

This work was supported by grants from the ARC Centre of Excellence in Plant Energy Biology (CE140100008), the ARC Centre of Excellence for Translational Photosynthesis (CE1401000015), the Australian Government National Collaborative Research Infrastructure Strategy (Australian Plant Phenomics Facility) – PIEPS grant, the International Wheat Yield Partnership and Grains Research Development Council Grant (ANU00027). We acknowledge the Endeavour Fellowship awarded to S.S. for which part of this research was developed.

CONFLICT OF INTEREST

The authors declare that they have no conflict of interest.

620 **REFERENCES**

621 Ainsworth E.A., Serbin S.P., Skoneczka J.A. & Townsend P.A. (2014) Using leaf optical
622 properties to detect ozone effects on foliar biochemistry. *Photosynthesis Research* 119,
623 65–76.

624 Appaix F., Minatchy M.N., Riva-Lavieille C., Olivares J., Antonsson B. & Saks V.A. (2000)
625 Rapid spectrophotometric method for quantitation of cytochrome *c* release from
626 isolated mitochondria or permeabilized cells revisited. *Biochimica et Biophysica Acta*
627 *(BBA)-Bioenergetics* 1457, 175–181.

628 Armstrong A.F., Logan D.C. & Atkin O.K. (2006a) On the developmental dependence of leaf
629 respiration: responses to short- and long-term changes in growth temperature. *American*
630 *Journal of Botany* 93, 1633–1639.

631 Armstrong A.F., Logan D.C., O'Toole P., Tobin A.K. & Atkin O.K. (2006b) Heterogeneity of
632 plant mitochondrial responses underpinning respiratory acclimation to the cold in
633 *Arabidopsis thaliana* leaves. *Plant, Cell & Environment* 29, 940–949.

634 Asner G.P. & Martin R.E. (2008) Spectral and chemical analysis of tropical forests: scaling
635 from leaf to canopy levels. *Remote Sensing of Environment* 112, 3958–3970.

636 Asner G.P., Martin R.E., Tupayachi R., Anderson C.B., Sinca F., Carranza-Jiménez L. &
637 Martinez P. (2014) Amazonian functional diversity from forest canopy chemical
638 assembly. *Proceedings of the National Academy of Sciences of the United States of*
639 *America* 111, 5604–5609.

640 Asner G.P., Martin R.E., Tupayachi R., Emerson R., Martinez P., Sinca F., …, Lugo A.E.
641 (2011) Taxonomy and remote sensing of leaf mass per area (LMA) in humid tropical
642 forests. *Ecological Applications* 21, 85–98.

643 Atkin O.K. & Tjoelker M.G. (2003) Thermal acclimation and the dynamic response of plant
644 respiration to temperature. *Trends in Plant Science* 8, 343–351.

645 Atkin O.K., Bloomfield K.J., Reich P.B., Tjoelker M.G., Asner G.P., Bonal D., …, Cosio E.G.
646 (2015) Global variability in leaf respiration in relation to climate, plant functional types
647 and leaf traits. *New Phytologist* 206, 614–636.
648 Atkin O.K., Scheurwater I. & Pons T.L. (2006) High thermal acclimation potential of both
649 photosynthesis and respiration in two lowland *Plantago* species in contrast to an alpine
650 congeneric. *Global Change Biology* 12, 500–515.
651 Atkin O.K., Scheurwater I. & Pons T.L. (2007) Respiration as a percentage of daily
652 photosynthesis in whole plants is homeostatic at moderate, but not high, growth
653 temperatures. *New Phytologist* 174, 367–380.
654 Barnes M.L., Breshears D.D., Law D.J., van Leeuwen W.J.D., Monson R.K., Fojtik A.C.,
655 Moore D.J.P. (2017) Beyond greenness: Detecting temporal changes in photosynthetic
656 capacity with hyperspectral reflectance data. *Plos One* 12, e0189539.
657 Beckmann K., Messinger J., Badger M.R., Wydrzynski T. & Hillier W. (2009) On-line mass
658 spectrometry: membrane inlet sampling. *Photosynthesis Research* 102, 511–522.
659 Blackburn G.A. (2007) Hyperspectral remote sensing of plant pigments. *Journal of*
660 *Experimental Botany* 58, 855–867.
661 Bolster K.L, Martin M.E. & Aber J.D. (1996) Determination of carbon fraction and nitrogen
662 concentration in tree foliage by near infrared reflectances: a comparison of statistical
663 methods. *Canadian Journal of Forest Research* 26, 590–600.
664 Bouma T.J., De Visser R., Van Leeuwen P.H., De Kock M.J. & Lambers H. (1995) The
665 respiratory energy requirements involved in nocturnal carbohydrate export from starch-
666 storing mature source leaves and their contribution to leaf dark respiration. *Journal of*
667 *Experimental Botany* 46, 1185–1194.
668 Breiman L. (2001) Random forests. *Machine Learning* 45, 5–32.

669 Byrd G.T., Sage R.F. & Brown R.H. (1992) A comparison of dark respiration between C_3 and
670 C_4 plants. *Plant Physiology* 100, 191–198.
671 Cassman K.G. (1999) Ecological intensification of cereal production systems: yield potential,
672 soil quality, and precision agriculture. *Proceedings of the National Academy of*
673 *Sciences of the United States of America* 96, 5952–5959.
674 Curran P.J. (1989) Remote sensing of foliar chemistry. *Remote Sensing of Environment* 30,
675 271–278.
676 Dechant B., Cuntz M., Vohland M., Schulz E., & Doktor D. (2017) Estimation of
677 photosynthesis traits from leaf reflectance spectra: Correlation to nitrogen content as
678 the dominant mechanism. *Remote Sensing of Environment* 196, 279–292.
679 Doughty C.E., Asner G.P. & Martin R.E. (2011) Predicting tropical plant physiology from leaf
680 and canopy spectroscopy. *Oecologia* 165, 289–299.
681 Ecarnot M., Compan F. & Roumet P. (2013) Assessing leaf nitrogen content and leaf mass per
682 unit area of wheat in the field throughout plant cycle with a portable spectrometer. *Field*
683 *Crops Research* 140, 44–50.
684 Evans J.R. (1989a) Photosynthesis and nitrogen relationships in leaves of C_3 plants. *Oecologia*
685 78, 9–19.
686 Evans J.R. (1989b) Partitioning of nitrogen between and within leaves grown under different
687 irradiances. *Functional Plant Biology* 16, 533–548.
688 Evans J.R. & Terashima I. (1988) Photosynthetic characteristics of spinach leaves grown with
689 different nitrogen treatments. *Plant and Cell Physiology* 29, 157–165.
690 Fan R., Sun J., Yang F., Li M., Zheng Y., Zhong Q. & Cheng D. (2017) Divergent scaling of
691 respiration rates to nitrogen and phosphorus across four woody seedlings between
692 different growing seasons. *Ecology and Evolution* 7, 8761–8769.

693 Feilhauer H., Asner G.P. & Martin R.E. (2015) Multi-method ensemble selection of spectral
694 bands related to leaf biochemistry. *Remote Sensing of Environment* 164, 57–65.
695 Field C. & Mooney H.A. (1986) The photosynthesis-nitrogen relationship in wild plants. In *On*
696 *the Economy of Form and Function.* (ed T.J. Givinsh), pp 25–55. Cambridge University
697 Press, Cambridge.
698 Furbank R.T., von Caemmerer S., Sheehy J. & Edwards G. (2009) C_4 rice: a challenge for plant
699 phenomics. *Functional Plant Biology* 36, 845–856.
700 Godfray H.C.J., Beddington J.R., Crute I.R., Haddad L., Lawrence D., Muir J.F., …, Toulmin
701 C. (2010) Food security: the challenge of feeding 9 billion people. *Science* 327, 812–
702 818.
703 Goldsmith P.D., Gunjal K. & Ndarishikanye B. (2004) Rural–urban migration and agricultural
704 productivity: the case of Senegal. *Agricultural Economics* 31, 33–45.
705 Guerrero C., Stenberg B., Wetterlind J., Viscarra Rossel R.A., Maestre F.T., Mouazen A.M.,
706 …, Kuang B. (2014) Assessment of soil organic carbon at local scale with spiked NIR
707 calibrations: effects of selection and extra-weighting on the spiking subset: Spiking and
708 extra-weighting to improve soil organic carbon predictions with NIR. *European*
709 *Journal of Soil Science* 65, 248–263.
710 Guerrero C., Wetterlind J., Stenberg B., Mouazen A.M., Gabarrón-Galeote M.A., Ruiz-Sinoga
711 J.D., …, Viscarra Rossel R.A. (2016) Do we really need large spectral libraries for local
712 scale SOC assessment with NIR spectroscopy? *Soil and Tillage Research* 155, 501–
713 509.
714 Guerrero C., Zornoza R., Gómez I. & Mataix-Beneyto J. (2010) Spiking of NIR regional
715 models using samples from target sites: Effect of model size on prediction accuracy.
716 *Geoderma* 158, 66–77.

717 Gutierrez M., Reynolds M.P. & Klatt A.R. (2010) Association of water spectral indices with
718 plant and soil water relations in contrasting wheat genotypes. *Journal of Experimental*
719 *Botany* 61, 3291–3303.
720 Hachiya T., Terashima I. & Noguchi K. (2007) Increase in respiratory cost at high growth
721 temperature is attributed to high protein turnover cost in *Petunia*× hybrida petals. *Plant,*
722 *Cell & Environment* 30, 1269–1283.
723 Harrison M.T., Edwards E.J., Farquhar G.D., Nicotra A.B. & Evans J.R. (2009) Nitrogen in
724 cell walls of sclerophyllous leaves accounts for little of the variation in photosynthetic
725 nitrogen-use efficiency. *Plant, Cell & Environment* 32, 259–270.
726 Hauben M., Haesendonckx B., Standaert E., Van Der Kelen K., Azmi A., Akpo H., …, Lambert
727 B. (2009) Energy use efficiency is characterized by an epigenetic component that can
728 be directed through artificial selection to increase yield. *Proceedings of the National*
729 *Academy of Sciences of the United States of America* 106, 20109–20114.
730 Heckmann D., Schlüter U. & Weber A.P. (2017) Machine learning techniques for predicting
731 crop photosynthetic capacity from leaf reflectance spectra. *Molecular Plant* 10, 878–
732 890.
733 Hirose T. & Werger M.J. (1987) Nitrogen use efficiency in instantaneous and daily
734 photosynthesis of leaves in the canopy of a *Solidago altissima* stand. *Physiologia*
735 *Plantarum* 70, 215–222.
736 Hoefnagel M.H.N. & Wiskich J.T. (1998) Activation of the plant alternative oxidase by high
737 reduction levels of the Q-Pool and pyruvate. *Archives of Biochemistry and Biophysics*
738 355, 262–270.
739 Hsu C.W., Chang C.C. & Lin C.J. (2003) A practical guide to support vector classification.
740 Technical Report, Department of Computer Science, National Taiwan University,

741 Taipei, Taiwan. pp 1–16. Retrieved from
742 http://www.csie.ntu.edu.tw/~cjlin/papers/guide/guide.pdf.
743 Hu Z., Vanderhaeghen R., Cools T., Wang Y., De Clercq I., Leroux O., …, Hilson P. (2016)
744 Mitochondrial defects confer tolerance against cellulose deficiency. *The Plant Cell* 28,
745 2276–2290.
746 Hurry V., Igamberdiev A.U., Keerberg O., Parnik T.R., Atkin O.K., Zaragoza‐Castells J., ⋯
747 , Ribas‐Carbó M. (2005). Respiration in photosynthetic cells: gas exchange
748 components, interactions with photorespiration and the operation of mitochondria in
749 the light. In *Plant respiration: from cell to ecosystem*. (eds H. Lambers & M. Ribas‐
750 Carbó), 18, 43–61. Springer, Dordrecht, The Netherlands.
751 IPCC (2013) Summary for policymakers. In *Climate Change 2013: The Physical Science*
752 *Basis. Contribution of Working Group I to the Fifth Assessment Report of the*
753 *Intergovernmental Panel on Climate Change* (eds T.F. Stocker, D. Qin, G.K. Plattner,
754 et al.), pp 3–29. Cambridge University Press, Cambridge.
755 Isbell R.F. (2002) The Australian Soil Classification. CSIRO Publishing: Collingwood.
756 Jacquemoud S. & Baret F. (1990) PROSPECT: A model of leaf optical properties spectra.
757 *Remote Sensing of Environment*, 34, 75–91.
758 Jacquemoud S., Ustin S.L., Verdebout J., Schmuck G., Andreoli G., & Hosgood B. (1996)
759 Estimating leaf biochemistry using the PROSPECT leaf optical properties model.
760 *Remote Sensing of Environment* 56, 194–202.
761 Jullien A., Allirand J.M., Mathieu A., Andrieu B. & Ney B. (2009) Variations in leaf mass per
762 area according to N nutrition, plant age, and leaf position reflect ontogenetic plasticity
763 in winter oilseed rape (*Brassica napus* L.). *Field Crops Research* 114, 188–197.
764 Kok B. (1948) A critical consideration of the quantum yield of *Chlorella*-photosynthesis.
765 *Enzymologia* 13, 1–56.

766 Laisk A.K. (1977) Kinetics of Photosynthesis and Photorespiration in C_3-plants. Nauka,
767 Moscow.
768 Lambers H., Chapin F.S. & Pons T.L. (2008) Plant Physiological Ecology. USA: Springer.
769 Loomis R.S. & Williams W.A. (1969) Productivity and the morphology of crop stands. In
770 *Physiological Aspects of Crop Yield* (eds J.D. Eastin, F.A. Haskin, C.Y. Sullivan, &
771 C.H.M. Van Bavel), pp 27–47. American Society of Agronomy, Winconsin.
772 Loreto F., Velikova V. & Di Marco G. (2001) Respiration in the light measured by CO_2-^{12}C
773 emission in CO_2-^{13}C atmosphere in maize leaves. *Australian Journal of Plant*
774 *Physiology* 28, 1103–1108.
775 Lusk C.H., Reich P.B., Montgomery R.A., Ackerly D.D. & Cavender-Bares J. (2008) Why are
776 evergreen leaves so contrary about shade? *Trends in Ecology & Evolution* 23, 299–303.
777 Makino Y., Ichimura M., Kawagoe Y. & Oshita S. (2007) Cytochrome *c* oxidase as a cause of
778 variation in oxygen uptake rates among vegetables. *Journal of the American Society for*
779 *Horticultural Science* 132, 239–245.
780 Makino Y., Ichimura M., Oshita S., Kawagoe Y. & Yamanaka H. (2010) Estimation of oxygen
781 uptake rate of tomato (*Lycopersicon esculentum* Mill.) fruits by artificial neural
782 networks modelled using near-infrared spectral absorbance and fruit mass. *Food*
783 *Chemistry* 121, 533–539.
784 Martin M.E. & Aber J.D. (1997) High spectral resolution remote sensing of forest canopy
785 lignin, nitrogen, and ecosystem processes. *Ecological Applications* 7, 431–443.
786 Martin A.R., Hale C.E., Cerabolini B.E., Cornelissen J.H., Craine J., Gough W.A., …, Tirona
787 CK. (2018) Inter-and intraspecific variation in leaf economic traits in wheat and maize.
788 *AoB Plants*, 10, p.ply006.

789 Mason M.G., Nicholls P. & Cooper C.E. (2014) Re-evaluation of the near infrared spectra of
790 mitochondrial cytochrome *c* oxidase: implications for non invasive *in vivo* monitoring
791 of tissues. *Biochimica et Biophysica Acta (BBA)-Bioenergetics* 1837, 882–1891.
792 Mevik B-H., Wehrens R., Liland K.H. (2016) pls: Partial Least Squares and Principal
793 Component Regression. R package version 2.6-0. https://CRAN.R-
794 project.org/package=pls
795 Meyer D., Dimitriadou E., Hornik K, Weingessel A., Leisch F. (2017) e1071: Misc Functions
796 of the Department of Statistics, Probability Theory Group (Formerly: E1071), TU
797 Wien. R package version 1.6-8. https://CRAN.R-project.org/package=e1071
798 Millar A.H., Whelan J., Soole K.L. & Day D.A. (2011) Organization and regulation of
799 mitochondrial respiration in plants. *Annual Review of Plant Biology* 62, 79–104.
800 Miroslavov E.A. & Kravkina I.M. (1991) Comparative analysis of chloroplasts and
801 mitochondria in leaf chlorenchyma from mountain plants grown at different altitudes.
802 *Annals of Botany* 68, 195–200.
803 Montesinos-López O.A., Montesinos-López A., Crossa J., los Campos G., Alvarado G.,
804 Suchismita M., …, Burgueño J. (2017a) Predicting grain yield using canopy
805 hyperspectral reflectance in wheat breeding data. *Plant Methods* 13, 4.
806 Montesinos-López A., Montesinos-López O.A., Cuevas J., Mata-López W.A., Burgueño J.,
807 Mondal S., …, Crossa J. (2017b) Genomic Bayesian functional regression models with
808 interactions for predicting wheat grain yield using hyper-spectral image data. *Plant*
809 *Methods* 13, 62.
810 Mooney H.A. (1963) Physiological ecology of coastal, subalpine, and alpine populations of
811 *Polygonum bistortoides*. *Ecology* 44, 812–816.

812 Noguchi K. (2005) Effects of light intensity and carbohydrate status on leaf and root
813 respiration. In *Plant Respiration from Cell to Ecosystem* (eds H. Lambers, & M. Ribas-
814 Carbo), pp 63–83. Springer, Dordrecht.
815 Noguchi K. & Yoshida K. (2008) Interaction between photosynthesis and respiration in
816 illuminated leaves. *Mitochondrion* 8, 87–99.
817 Oleksyn J., Modrzynski J., Tjoelker M.G., Zytkowiak R., Reich P.B. & Karolewski P. (1998)
818 Growth and physiology of *Picea abies* populations from elevational transects: common
819 garden evidence for altitudinal ecotypes and cold adaptation. *Functional Ecology* 12,
820 573–590.
821 O'Leary B.M., Lee C.P., Atkin O.K., Cheng R., Brown T.B. & Millar A.H. (2017) Variation
822 in leaf respiration rates at night correlates with carbohydrate and amino acid supply.
823 *Plant Physiology* 174, 2261–2273.
824 Pärnik T., & Keerberg O. (1995) Decarboxylation of primary and end products of
825 photosynthesis at different oxygen concentrations. *Journal of Experimental Botany* 46,
826 1439–1447.
827 Parry M.A.J., Madgwick P.J., Carvalho J.F.C. & Andralojc P.J. (2007) Prospects for increasing
828 photosynthesis by overcoming the limitations of Rubisco. *The Journal of Agricultural*
829 *Science* 145, 31.
830 Peraudeau S., Lafarge T., Roques S., Quiñones C.O., Clement-Vidal A., Ouwerkerk P.B., …,
831 Dingkuhn M. (2015) Effect of carbohydrates and night temperature on night respiration
832 in rice. *Journal of Experimental Botany* 66, 3931–3944.
833 Poorter H., Niinemets U., Poorter L., Wright I.J. & Villar R. (2009) Causes and consequences
834 of variation in leaf mass per area (LMA): a meta-analysis. *New Phytologist* 183, 565–
835 588.

836 Poorter H., Remkes C. & Lambers H. (1990) Carbon and nitrogen economy of 24 wild species
837 differing in relative growth rate. *Plant Physiology* 94, 621–627
838 R Core Team (2018). R: A language and environment for statistical computing. R Foundation
839 for Statistical Computing, Vienna, Austria. URL https://www.R-project.org/.
840 Ramirez J.A., Posada J.M., Handa I.T., Hoch G., Vohland M., Messier C., & Reu B. (2015)
841 Near-infrared spectroscopy (NIRS) predicts non-structural carbohydrate concentrations
842 in different tissue types of a broad range of tree species. *Methods in Ecology and*
843 *Evolution* 6, 1018–1025.
844 Reich P.B., Tjoelker M.G., Pregitzer K.S., Wright I.J., Oleksyn J. & Machado J.L. (2008)
845 Scaling of respiration to nitrogen in leaves, stems and roots of higher land plants.
846 *Ecology Letters* 11, 793–801.
847 Reich P.B. & Walters M.B. (1994) Photosynthesis-nitrogen relations in Amazonian tree
848 species. II. Variation in nitrogen vis-a-vis specific leaf area influences mass- and area-
849 based expressions. *Oecologia* 97, 73–81
850 Reich P.B., Walters M.B. & Ellsworth D.S. (1997) From tropics to tundra: global convergence
851 in plant functioning. *Proceedings of the National Academy of Sciences of the United*
852 *States of America* 94, 13730–13734.
853 Reich P.B., Walters M.B., Ellsworth D.S., Vose J.M., Volin J.C., Gresham C. & Bowman W.D.
854 (1998a) Relationships of leaf dark respiration to leaf nitrogen, specific leaf area and
855 leaf life-span: a test across biomes and functional groups. *Oecologia* 114, 471–482.
856 Reich P.B., Walters M.B., Tjoelker M., Vanderklein D. & Buschena C. (1998b) Photosynthesis
857 and respiration rates depend on leaf and root morphology and nitrogen concentration in
858 nine boreal tree species differing in relative growth rate. *Functional Ecology* 12, 395–
859 405.

860 Ryan M.G. (1991) Effects of climate change on plant respiration. *Ecological Applications* 1,
861 157–167.
862 Scafaro A.P., Negrini A.C.A., O'Leary B., Rashid F.A.A., Hayes L., Fan Y., …, Atkin O.K.
863 (2017) The combination of gas-phase fluorophore technology and automation to enable
864 high-throughput analysis of plant respiration. *Plant Methods* 13, 16.
865 Serbin S.P., Dillaway D.N., Kruger E.L. & Townsend P.A. (2012) Leaf optical properties
866 reflect variation in photosynthetic metabolism and its sensitivity to temperature.
867 *Journal of Experimental Botany* 63, 489–502.
868 Sew Y.S., Ströher E., Holzmann C., Huang S., Taylor N.L., Jordana X. & Millar A.H. (2013)
869 Multiplex micro-respiratory measurements of Arabidopsis tissues. *New Phytologist*
870 200, 922–932.
871 Silva-Pérez V., Molero G., Serbin S.P., Condon A.G., Reynolds M.P., Furbank R.T. & Evans
872 J.R. (2018) Hyperspectral reflectance as a tool to measure biochemical and
873 physiological traits in wheat. *Journal of Experimental Botany* 69, 483–496.
874 Sims D.A & Gamon J.A. (2003) Estimation of vegetation water content and photosynthetic
875 tissue area from spectral reflectance: a comparison of indices based on liquid water and
876 chlorophyll absorption features. *Remote Sensing of Environment* 84, 526–537.
877 Thissen U., Pepers M., Üstün B., Melssen W.J. & Buydens L.M.C. (2004) Comparing support
878 vector machines to PLS for spectral regression applications. *Chemometrics and*
879 *Intelligent Laboratory Systems* 73, 169–179.
880 Tilman D., Balzer C., Hill J. & Befort B.L. (2011) Global food demand and the sustainable
881 intensification of agriculture. *Proceedings of the National Academy of Sciences of the*
882 *United States of America* 108, 20260–20264.
883 Tilman D., Cassman K.G., Matson P.A., Naylor R. & Polasky S. (2002) Agricultural
884 sustainability and intensive production practices. *Nature* 418, 671–677.

885 Umbach A.L., Lacey E.P. & Richter S.J. (2009). Temperature-sensitive alternative oxidase
886 protein content and its relationship to floral reflectance in natural *Plantago lanceolata*
887 populations. *New Phytologist* 181, 662–671.
888 United Nations Department of Economic and Social Affairs Population Division (2015) World
889 population prospects: The 2015 revision, methodology of the United Nations
890 population estimates and projections. Working Paper No. ESA/P/WP.242. United
891 Nations, New York.
892 Vanlerberghe G.C. & McIntosh L. (1997) Alternative oxidase: from gene to function. *Annual*
893 *Review of Plant Biology* 48, 703–734.
894 Vapnik V.N. (1995) The Nature of Statistical Learning Theory. Springer-Verlag Inc.: New
895 York.
896 Weber V.S., Araus J.L., Cairns J.E., Sanchez C., Melchinger A.E. & Orsini E. (2012)
897 Prediction of grain yield using reflectance spectra of canopy and leaves in maize plants
898 grown under different water regimes. *Field Crops Research* 128, 82–90.
899 Wilson D. & Jones J.G. (1982) Effect of selection for dark respiration rate of mature leaves on
900 crop yields of *Lolium perenne* cv. S23. *Annals of Botany* 49, 313–320.
901 Wold S., Sjöström M. & Eriksson L. (2001) PLS-regression: a basic tool of chemometrics.
902 *Chemometrics and Intelligent Laboratory Systems* 58, 109–130.
903 Wright I.J., Reich P.B., Atkin O.K., Lusk C.H., Tjoelker M.G. & Westoby M. (2006)
904 Irradiance, temperature and rainfall influence leaf dark respiration in woody plants:
905 evidence from comparisons across 20 sites. *New Phytologist* 169, 309–319.
906 Wright I.J., Reich P.B., Westoby M., Ackerly D.D., Baruch Z., Bongers F., …, Villar R. (2004)
907 The worldwide leaf economics spectrum. *Nature* 428, 821.
908 Xiao Z. & Ximing C. (2011) Climate change impacts on global agricultural land availability.
909 *Environmental Research Letters* 6, 014014.

910 Xiang S., Reich P.B., Sun S. & Atkin O.K. (2013) Contrasting leaf trait scaling relationships
911 in tropical and temperate wet forest species. *Functional Ecology* 27, 522–534.
912 Yendrek C.R., Tomaz T., Montes C.M., Cao Y., Morse A.M., Brown P.J., …, Ainsworth EA.
913 (2017) High-throughput phenotyping of maize leaf physiological and biochemical traits
914 using hyperspectral reflectance. *Plant Physiology* 173, 614–626.
915 Zadoks J.C., Chang T.T. & Konzak C.F. (1974) A decimal code for the growth stages of
916 cereals. *Weed Research* 14, 415–421.

TABLE 1 Materials and growth environment for the different experiments

Experiment	Location	Genotypes†	Zadoks growth scale‡	Leaf sampled	Day/night temperature (˚C)	Light (PPFD§, µmol m^{-2} s^{-1}), photoperiod
1	ANU¶	3	13	Third true leaf (Leaf-3)	21/16, 28/23 or 35/30	600~800 or 150~200, 12 h
2	ANU¶	70	13, and 61-69	Leaf-3, leaf subtending the flag leaf (Flag-1) and flag leaf	25/20	400~1200, 10-12 h day^{-1}
3	CSIRO[5ǂ]	24	23-27, and 55-71	Leaf subtending Flag-1, Flag-1 and flag leaf	27/12	---, 12-14 h day^{-1}

†A list is provided in Table S1; ‡Zadoks et al. (1974); §Photosynthetic photon flux density; ¶Glasshouse at Controlled Environment Facilities, Research School of Biology, Australian National University, Canberra, Australia; ǂPolytunnel at CSIRO Ginninderra Field Station, North Canberra, Australia; --- data not available.

TABLE 2 Variation in leaf dark respiration (R_{dark}, per square metre of leaf area (LA), per gram of fresh mass (FM), dry mass (DM), or leaf nitrogen (N)), nitrogen (per gram of DM, N_{mass}, or per square metre of LA, N_{area}), and leaf mass per area (LMA) of wheat genotypes.

	Experiment 1		Experiment 2		Experiment 3		All Experiments
Trait	**Range**	**Mean±SD**[†]	**Range**	**Mean±SD**	**Range**	**Mean±SD**	**Mean (CV**[‡]**)**
Leaf R_{dark} per unit							
LA (μmol O_2 m_{LA}^{-2} s^{-1})	0.18- 1.04	0.50± 0.18	0.28- 1.27	0.72± 0.18	0.26- 1.27	0.83± 0.21	0.73 (0.28)
FM (nmol O_2 g_{FM}^{-1} s^{-1})	0.82- 5.24	2.62± 0.88	1.66- 7.33	4.10± 1.07	1.19- 7.25	4.30± 1.12	4.05 (0.29)
DM (nmol O_2 g_{DM}^{-1} s^{-1})	5.26- 32.05	17.96± 4.61	7.66- 37.38	22.37± 6.09	5.17- 35.40	19.22± 5.67	21.05 (0.29)
N (nmol O_2 g_N^{-1} s^{-1})	86.6-540.4	293.7± 86.4	149.4-675.6	403.7± 85.2	144.0-1260.5	599.5± 226.4	448.5 (0.37)
Other leaf traits							
N_{mass} (mg g^{-1})	53.8- 71.3	61.8± 3.5	33.6- 77.1	55.8±10.2	17.3-64.6	34.1± 7.8	49.5 (0.28)
N_{area} (g m^{-2})	0.50- 1.41	0.86±0.20	0.48- 1.44	0.94±0.17	0.32-1.44	0.74±0.23	0.87 (0.21)
LMA (g m^{-2})	16.9- 41.7	27.0± 6.2	17.2- 57.8	33.0± 7.8	14.2-59.0	29.7±11.6	31.5 (0.29)

[†]SD, standard deviation; [‡]CV, coefficient of variation; n=105-107, 815-840, and 398-423 for Experiments 1, 2 and 3 respectively.

TABLE 3 Pearson correlation coefficients matrix for leaf dark respiration (R_{dark}, per square metre of leaf area (LA), per gram of fresh mass (FM), dry mass (DM), or leaf nitrogen (N)), nitrogen (per gram of DM, N_{mass}, or per square metre of LA, N_{area}), and leaf mass per area (LMA) of all three experiments.

Trait	**Leaf R_{dark} per unit**				**N_{mass}**	**N_{area}**
	LA (μmol O_2 m_{LA}^{-2} s^{-1})	**FM (nmol O_2 g_{FM}^{-1} s^{-1})**	**DM (nmol O_2 g_{DM}^{-1} s^{-1})**	**N (nmol O_2 g_N^{-1} s^{-1})**	**(mg g^{-1})**	**(g m^{-2})**
R_{dark} per unit LA						
R_{dark} per unit FM	0.881***					
R_{dark} per unit DM	0.529***	0.451***				
R_{dark} per unit N	0.684***	0.587***	0.457***			
N_{mass}	-0.290***	-0.270***	0.377***	-0.592***		
N_{area}	0.159***	0.219***	0.178***	-0.307***	0.494***	
LMA	0.268***	0.347**	-0.080**	0.111***	-0.230***	0.118***

Values are Pearson's *p*. *P*<0.05, 0.01, and 0.001 are indicated by *, **, and *** respectively.

928 **Table 4** Summary of PLSR and SVMR model performance for prediction of leaf dark respiration (R_{dark}, expressed per square metre of leaf area
929 (LA), per gram of fresh mass (FM), per gram dry mass (DM) and per gram leaf nitrogen (N)) and other target traits, including leaf nitrogen
930 (expressed per gram of DM and per square metre of LA), and leaf mass per unit area (LMA) across all experiments.

	Coefficient of determination (r^2)		Root mean square error (RMSE)		Relative bias (%)	
All Experiment[†]	**PLSR (NC**[‡]**)**	**SVRM**	**PLSR**	**SVRM**	**PLSR**	**SVRM**
R_{dark} LA (μmol O_2 m_{LA}^{-2} s^{-1})	0.54 (23)	0.53	0.14	0.15	16.7	15.5
R_{dark} FM (nmol O_2 g_{FM}^{-1} s^{-1})	0.55 (24)	0.53	0.79	0.80	17.0	18.1
R_{dark} DM (nmol O_2 g_{DM}^{-1} s^{-1})	0.50 (23)	0.48	4.34	4.87	17.4	16.7
R_{dark} N (nmol O_2 g_N^{-1} s^{-1})	0.63 (18)	0.64	102.4	103.8	18.2	17.0
N_{mass} (mg g^{-1})	0.91 (26)	0.90	4.15	4.35	7.1	8.0
N_{area} (g m^{-2})	0.60 (18)	0.62	0.13	0.13	11.8	11.1
LMA (g m^{-2})	0.75 (14)	0.72	4.53	5.05	11.3	10.8

931 [†]Models were built on training datasets consisting of 90% of the experimental data and used to predict the remaining (test dataset of) 10%.
932 [‡]Number of components used.

FIGURE LEGENDS

FIGURE 1 Mean (± standard deviation), minimum and maximum leaf reflectance **(a)** of wheat and spectral coefficients of variation **(b)** for three experiments (Experiments 1, 2 and 3) combined.

FIGURE 2 Relationships between R_{dark_LA} and **(a)** nitrogen content per unit leaf area (N_{area}), **(b)** leaf dry mass per unit leaf area (LMA), and **(c)** between R_{dark_DM} and nitrogen concentration per unit leaf dry mass (N_{mass}). Pearson correlation coefficients (r) for data pooled from Experiments 1, 2 and 3 are presented in the plots. For each of Experiment 1 (red circles), Experiment 2 (blue triangles) and Experiment 3 (purple squares) the respective r were -0.36, 0.36 and 0.40 for R_{dark_LA} vs N_{area}, -0.37, 0.33 and 0.33 for R_{dark_LA} vs LMA, and -0.20, 0.63 and -0.10 for R_{dark_DM} vs N_{mass}.

FIGURE 3 Relationship between nitrogen content per unit leaf area (N_{area}) and leaf dry mass per unit leaf area (LMA) for all three experiments combined. Pearson correlation coefficients (r) for each of Experiment 1 (red circles), Experiment 2 (blue triangles) and Experiment 3 (purple squares) were 0.78, 0.22 and -0.19, respectively. For all bivariate relationships between traits across all experiments, see Table 3.

FIGURE 4 Validation of PLSR model prediction for R_{dark_LA} **(a)**, R_{dark_FM} **(b)**, R_{dark_DM} **(c)** and R_{dark_N} **(d)** using 10% of pooled data from Experiment 1 (red circles), Experiment 2 (blue triangles) and Experiment 3 (purple squares) that were not used in developing the model.

FIGURE 5 Validation of PLSR model prediction for nitrogen concentration per unit leaf dry mass (N_{mass}; **a**), nitrogen content per unit leaf area (N_{area}; **b**) and leaf dry mass per unit area (LMA; **c**), using 10% of pooled data from Experiment 1 (red circles), Experiment 2 (blue triangles) and Experiment 3 (purple squares) that were not used in developing the model.

FIGURE 6 Coefficient of determination (r^2) of PLSR models used for prediction of leaf dark respiration expressed per square metre of leaf area ($R_{dark\_LA;}$ **a**), per gram of fresh mass (R_{dark_FM}; **b**), per gram of dry mass (R_{dark_DM}; **c**), or per gram of leaf nitrogen (R_{dark_N}; **d**). PLSR models were trained on 90% of data pooled from Experiments 1, 2 and 3 (black bars) or Experiments 1 and 2 (grey bars) or from individual experiments (Experiment 1 (vertical stripped bars), Experiment 2 (white bars), or Experiment 3 (dotted bars)) and validated on the test dataset (remaining 10%). See Fig S5 for root mean squared error of PLSR models for predictions of same traits.

FIGURE 7 Coefficient of determination (r^2) of PLSR modesl used for prediction of leaf nitrogen expressed per gram of DM (N_{mass}; **a**) or per square metre of LA (N_{area}; **b**), and LMA (**c**). PLSR models were trained on 90% of data pooled from Experiments 1, 2 and 3 (black bars) or Experiments 1 and 2 (grey bars) or from individual experiments (Experiment 1 (vertical stripped bars), Experiment 2 (white bars), or Experiment 3 (dotted bars)) and validated on the test dataset (remaining 10%). See Fig S6 for root mean squared error of PLSR models for predictions of same traits.

971 **Title**

972 Predicting dark respiration rates of wheat leaves from hyperspectral reflectance

973

974 **Running Title**

975 Spectral reflectance for predicting leaf respiration

976

977 **Supporting Information**

978 **Table S1** Genotypes used for study.

	Experiment 1	Experiment 2	Experiment 3
1	Calingiri[†]	39586	Axe[§]
2	Halberd or Halgerg[†, ‡]	39592	CCG2
3	Janz[†]	39606	CCG4
4		39608	CCG5
5		39611	CCG6
6		39636	CCG7
7		705-WW	CCG10
8		803-WW	CCG11
9		93-WW	CCG13
10		959WW	CCG14
11		Annuello	CCG15
12		Aroona	CCG16
13		Arrino	CCG18
14		Axe[§]	CCG19
15		Baxter	CCG22
16		Berkut	CCG23
17		Binno or Binnu [‡]	CCG24
18		BT-schomburgk	CCG25
19		Bumper	CCG26
20		Calingiri[†]	CCG28
21		Carnamah	Drysdale[§]
22		Cascades	Espada[§]
23		Catalina	Maxe[§]
24		Chara-WT	Magenta[§]
25		Clearfield STL	
26		Correli or Corrill [‡]	
27		Cranbrook	
28		Datatine	
29		DM-WW	
30		Drysdale[§]	
31		Ducula 4	

32	EGA-Bonnie Rock
33	EGA-Eagle Rock
34	EGA-2248
35	Endure
36	Espada[§]
37	Excalibur
38	Fang
39	Fortune
40	Frame
41	GBA sapphire
42	Gladius
43	Guardian
44	H45
45	Halgerg or Halberd[†, ‡]
46	Hartog
47	Janz[†]
48	Krichau ff
49	Lang
50	Lincoln
51	Mace[§]
52	Machete
53	Magenta[†]
54	Magenta
55	Perenjori
56	Rees
57	Ruby
58	Sarc 1
59	Spear
60	Stiletto
61	Sunco
62	Tamamrin Rock or Tammarin_Rock[‡]
63	Ventura
64	Wentworth
65	Westoria
66	Wyalkatchem
67	Yaradouka or Yanadouka[‡]
68	Yipti
69	Young
70	Zippy

[†]Genotypes common to Experiments 1 and 2; [‡]Alternative spelling; [§]Genotypes common to Experiments 2 and 3.

Table S2 Foliar traits of wheat genotypes for Experiment 1 under different growth irradiance and temperature conditions averaged for three cultivars.

Irradiance /temperature (T)	Leaf R_{dark} per unit[†]				N_{mass}[‡] (mg g^{-1})	N_{area} (g m^{-2})	LMA[§] (g m^{-2})
	LA (μmol O_2 m_{LA}^{-2} s^{-1})	FM (nmol O_2 g_{FM}^{-1} s^{-1})	DM (nmol O_2 g_{DM}^{-1} s^{-1})	N (nmol O_2 g_N^{-1} s^{-1})			
High light							
21/16°C	0.62	2.84	19.52	311.2	63.4	0.87	25.9
28/23°C	0.57	2.77	18.27	297.0	63.4	0.84	28.2
35/30°C	0.64	3.24	18.02	301.6	60.3	0.84	26.4
Low light							
21/16°C	0.33	1.96	16.37	270.0	61.3	0.87	27.0
28/23°C	0.43	2.63	20.28	336.3	61.1	0.84	27.1
35/30°C	0.37	2.24	15.23	247.0	61.1	0.88	27.3
LSD							
Irradiance	0.04***	0.26***	1.62^{ns}	28.6^{ns}	1.2$^{P=0.063}$	0.08^{ns}	2.4^{ns}
T	0.05^{ns}	0.32^{ns}	1.99*	35.0$^{P=0.051}$	1.5$^{P=0.059}$	0.10^{ns}	3.0^{ns}
Irradiance * T	0.08**	0.45*	2.81*	49.5*	2.1$^{P=0.063}$	0.14^{ns}	4.2^{ns}

[†]Leaf R_{dark} values are expressed per unit leaf area (LA, μmol O_2 m_{LA}^{-2} s^{-1}), fresh mass (FM, nmol O_2 g_{FM}^{-1} s^{-1}), dry mass (DM, nmol O_2 g_{DM}^{-1} s^{-1}), nitrogen (N, nmol O_2 g_N^{-1} s^{-1}); [‡]N is expressed per gram of DM and per metre of LA; [§]LMA, leaf mass per area; LSD=Least significant difference; ns=not significant (P>0.05); P<0.05, 0.01, and 0.001 are indicated by *, **, and *** respectively; n=105-107.

Table S3 Means, mean squares and *F*. probabilities of ANOVAs for foliar traits examined during Experiments 2 for different genotypes and at different growth stages (GS).

Treatment		Leaf R_{dark} per unit†				N_{mass}‡ (mg g^{-1})	N_{area} (g m^{-2})	LMA§ (g m^{-2})
	d.f.	LA (µmol O_2 m_{LA}^{-2} s^{-1})	FM (nmol O_2 g_{FM}^{-1} s^{-1})	DM (nmol O_2 g_{DM}^{-1} s^{-1})	N (nmol O_2 g_N^{-1} s^{-1})			
Growth stage¶								
Vegetative stage		0.76	3.99	28.77	392.4	68.3	1.02	25.8
Reproductive stage		0.70	4.16	19.33	426.7	49.5	0.90	36.6
LSD $_{(P<0.05)}$		0.03	0.15	0.62	12.0	0.7	0.02	0.8
Mean squares and F. probabilities of ANOVA								
Genotype	69	0.08***	3.09***	35.6***	6005^{ns}	63.4***	0.04***	80.0***
GS	1	0.58***	6.42***	16319.7***	219939***	64892.5***	2.52***	21537.5***
Genotype*GS	69	$0.03^{P=0.053}$	$1.10^{P=0.06}$	21.4**	4806^{ns}	33.24***	0.06***	23.7^{ns}
Residual[3]		0.02 (689)	0.85 (690)	14.3 (679)	6551	18.82 (690)	0.02 (679)	27.1 (694)

†Leaf R_{dark} expressed per unit leaf area (LA, µmol O_2 m_{LA}^{-2} s^{-1}), fresh mass (FM, nmol O_2 g_{FM}^{-1} s^{-1}), dry mass (DM, nmol O_2 g_{DM}^{-1} s^{-1}) and nitrogen (N, nmol O_2 g_N^{-1} s^{-1}); ‡N is expressed per gram of DM and per metre of LA; §LMA, leaf mass per area; ¶Vegetative stage being leaf-3 at growth stage Z13 (seedling growth) while reproductive stage being flag leaf and Flag-1 at growth stages Z61-69 (anthesis). Values in parenthesis are residual degrees of freedom; ns=not significant ($P>0.05$); $P<0.05$, 0.01, and 0.001 are indicated by *, **, and *** respectively.

Table S4 Means, mean squares and *F*. probabilities of ANOVAs for foliar traits examined during Experiments 3 for different genotypes and at different growth stages (GS).

Treatment	d.f.	Leaf R_{dark} per unit[†] LA ($\mu mol\ O_2\ m_{LA}^{-2}\ s^{-1}$)	FM ($nmol\ O_2\ g_{FM}^{-1}\ s^{-1}$)	DM ($nmol\ O_2\ g_{DM}^{-1}\ s^{-1}$)	N ($nmol\ O_2\ g_N^{-1}\ s^{-1}$)	N_{mass}[‡] ($mg\ g^{-1}$)	N_{area} ($g\ m^{-2}$)	LMA[§] ($g\ m^{-2}$)
Growth stage[¶]								
Vegetative stage		0.89	4.62	22.40	491.9	32.7	0.66	40.1
Reproductive stage		0.76	3.97	16.18	708.1	35.5	0.82	19.4
LSD $_{(P<0.05)}$		0.04	0.21	0.91	40.0	1.5	0.04	1.0
Mean squares and F. probabilities of ANOVA								
Genotype	23	0.06 $^{P=0.064}$	1.24^{ns}	28.8^{ns}	32796^{ns}	116.5***	0.10***	26.8^{ns}
GS	1	1.87***	45.02***	4058.0***	4852040***	820.8***	2.69***	45082.8***
Genotype*GS	23	0.02^{ns}	0.47^{ns}	18.5^{ns}	25601^{ns}	40.3^{ns}	0.02^{ns}	21.1^{ns}
Residual		0.04 (364)	1.18 (370)	21.8 (367)	38343	49.9 (373)	0.04 (368)	28.6 (373)

[†]Leaf R_{dark} expressed per unit leaf area (LA, $\mu mol\ O_2\ m_{LA}^{-2}\ s^{-1}$), fresh mass (FM, $nmol\ O_2\ g_{FM}^{-1}\ s^{-1}$), dry mass (DM, $nmol\ O_2\ g_{DM}^{-1}\ s^{-1}$) and nitrogen (N, $nmol\ O_2\ g_N^{-1}\ s^{-1}$); [‡]N is expressed per gram of DM and per metre of LA; [§]LMA, leaf mass per area; ¶Vegetative stage being leaf-3 through leaf-6 sampled at growth stages Z23-27 (tillering) while reproductive stage being flag leaf, Flag-1 at growth stages Z55-71 (inflorescence emergence, anthesis through milk development). Values in parenthesis are residual degrees of freedom; ns=not significant ($P>0.05$); $P<0.05$, 0.01, and 0.001 are indicated by *, **, and *** respectively.

Table S5 Squared Pearson correlation (r^2) for predictions of leaf dark respiration (R_{dark}, expressed per metre of leaf area (LA), per gram of fresh mass (FM) and dry mass (DM), and leaf nitrogen), nitrogen (expressed per gram of DM and per metre of LA), and leaf mass per unit area (LMA), across all experiments, by the three models using either the continuous, full-spectrum data (350-2500 nm) or a spectral subset selected based on coefficient weightings of a multi-method ensemble developed by Feilhauer et al. (2015).

All Experiment[†]	PLSR		RFR		SVMR		Number of ensemble selected wavelengths
	Whole spectrum	Selected wavelengths	Whole spectrum	Selected wavelengths	Whole spectrum	Selected wavelengths	
Leaf R_{dark} per unit							
LA ($\mu mol\ O_2\ m_{LA}^{-2}\ s^{-1}$)	0.52	0.55	0.40	0.41	0.56	0.54	265
FM ($nmol\ O_2\ g_{FM}^{-1}\ s^{-1}$)	0.52	0.54	0.43	0.44	0.55	0.55	269
DM ($nmol\ O_2\ g_{DM}^{-1}\ s^{-1}$)	0.42	0.51	0.45	0.50	0.51	0.57	248
N ($nmol\ O_2\ g_N^{-1}\ s^{-1}$)	0.59	0.64	0.60	0.60	0.63	0.68	243
Other traits							
N_{mass} ($mg\ g^{-1}$)	0.81	0.84	0.80	0.80	0.84	0.85	229
N_{area} ($g\ m^{-2}$)	0.58	0.66	0.56	0.55	0.63	0.68	228
LMA ($g\ m^{-2}$)	0.69	0.79	0.71	0.70	0.76	0.80	221

[†]Models were built on training dataset consisting of 90% of the experimental data and used to predict the remaining (test dataset of) 10%.

Table S6. Summary of different trait-based and reflectance-based regression models for leaf dark respiration expressed per square metre of leaf area (R_{dark} LA). Model predictors are either reflectance, or measured leaf traits – leaf nitrogen (expressed per gram of DM, N_{mass}; and per metre of LA, N_{area}), and leaf mass per unit area (LMA). The coefficient of determination, R^2, is shown for all models.

Predictor(s)	Method	R_{dark} LA coefficient of determination (R^2)
Advanced regression		
Reflectance	PLSR	**0.54**
	SVMR	0.53
Traditional regression		
N_{mass}	Simple linear regression	0.08
N_{area}	Simple linear regression	0.04
LMA	Simple linear regression	0.07
N_{mass}, LMA	Multiple linear regression, no interaction	0.12
	Multiple linear regression, with interaction	0.12
N_{area}, LMA	Multiple linear regression, no interaction	0.09
	Multiple linear regression, with interaction	0.09

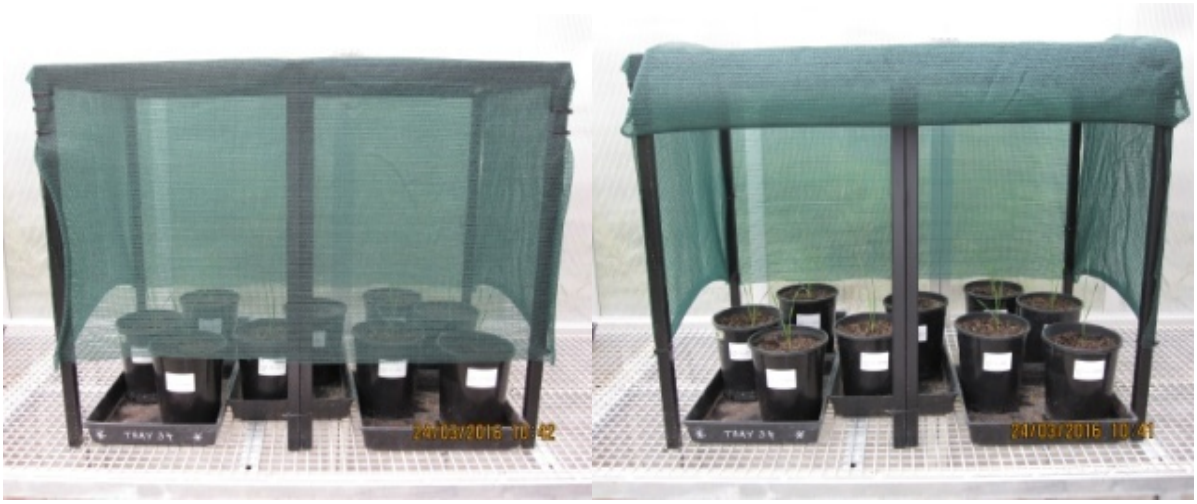

FIGURE S1 Display showing green mesh suspended by metal cages used to achieve low light (photosynthetic photon flux density of 150~200 µmol m^{-2} s^{-1} i.e. 25% of ambient) intensity during Experiment 1.

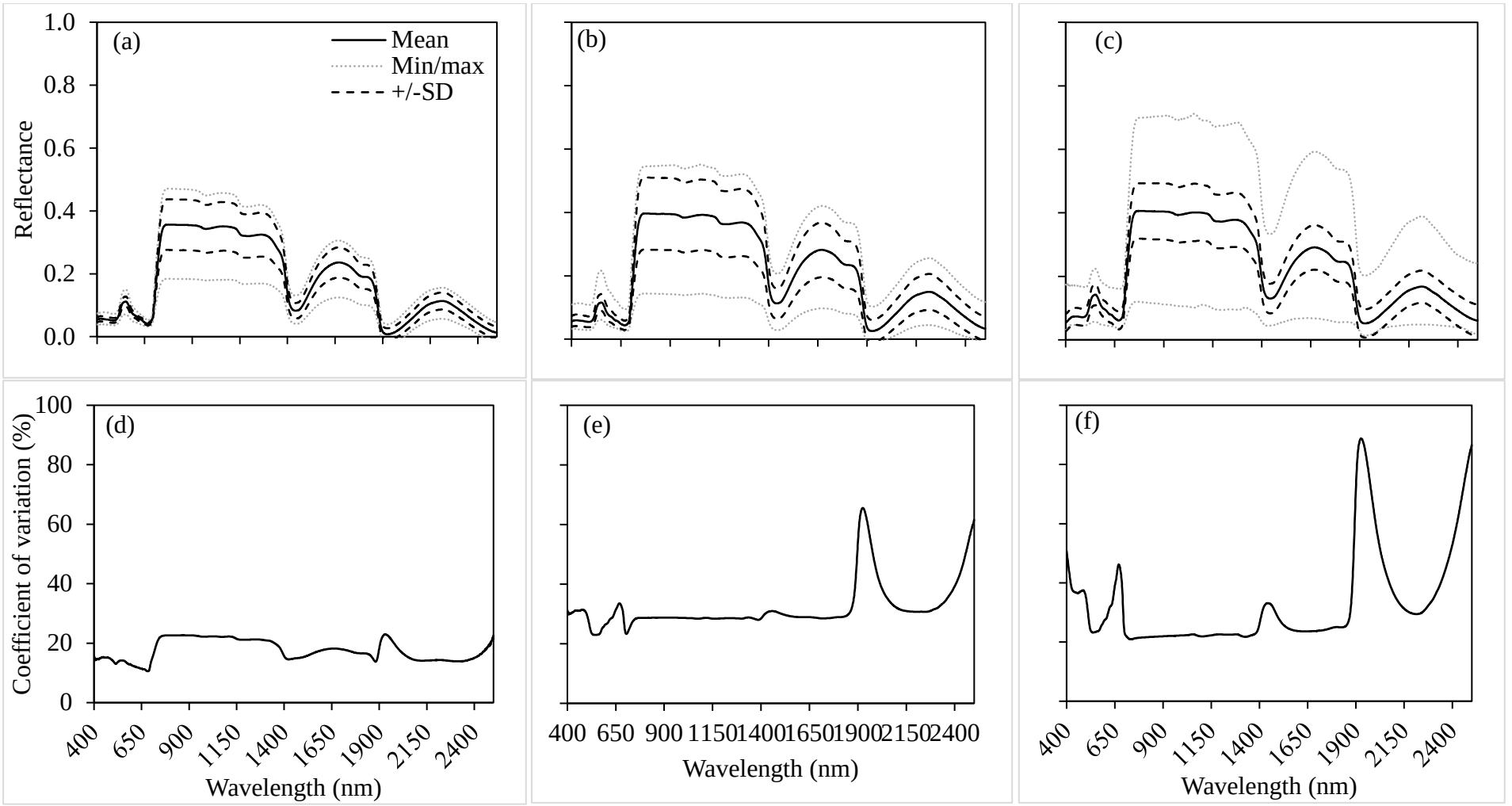

FIGURE S2 Mean (± standard deviation), minimum and maximum leaf reflectance (top panels) of wheat **(a-c)** and spectral coefficients of variation **(d-e)** for Experiment 1 (left panels), Experiment 2 (middle panels) and Experiment 3 (right panels).

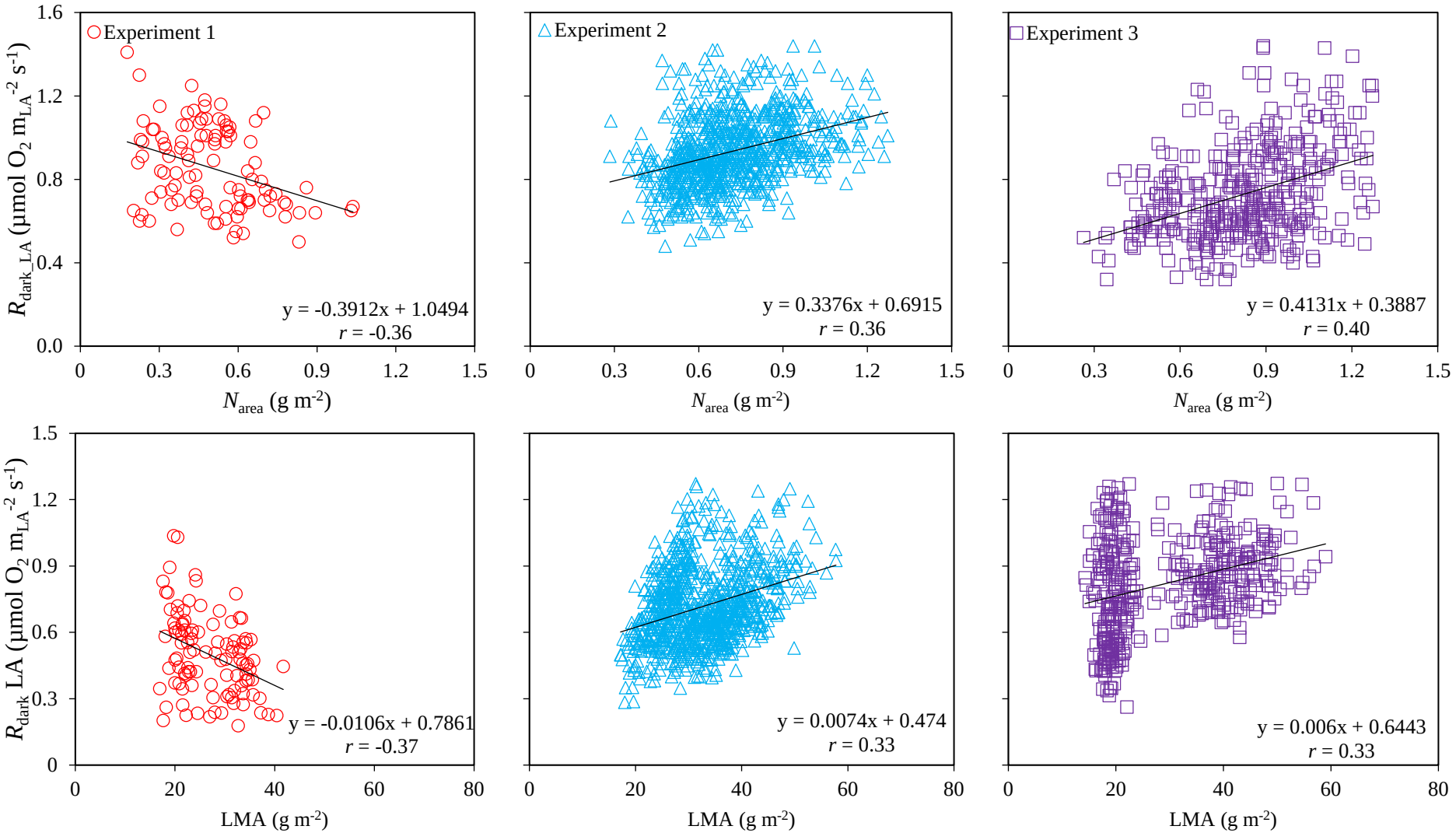
Experiment 1
y = -0.3912x + 1.0494
r = -0.36
Experiment 2
y = 0.3376x + 0.6915
r = 0.36
Experiment 3
y = 0.4131x + 0.3887
r = 0.40
Rdark_LA (μmol O2 mLA-2 s-1)
Narea (g m-2)
y = -0.0106x + 0.7861
r = -0.37
y = 0.0074x + 0.474
r = 0.33
y = 0.006x + 0.6443
r = 0.33
Rdark LA (μmol O2 mLA-2 s-1)
LMA (g m-2)

22

23
24

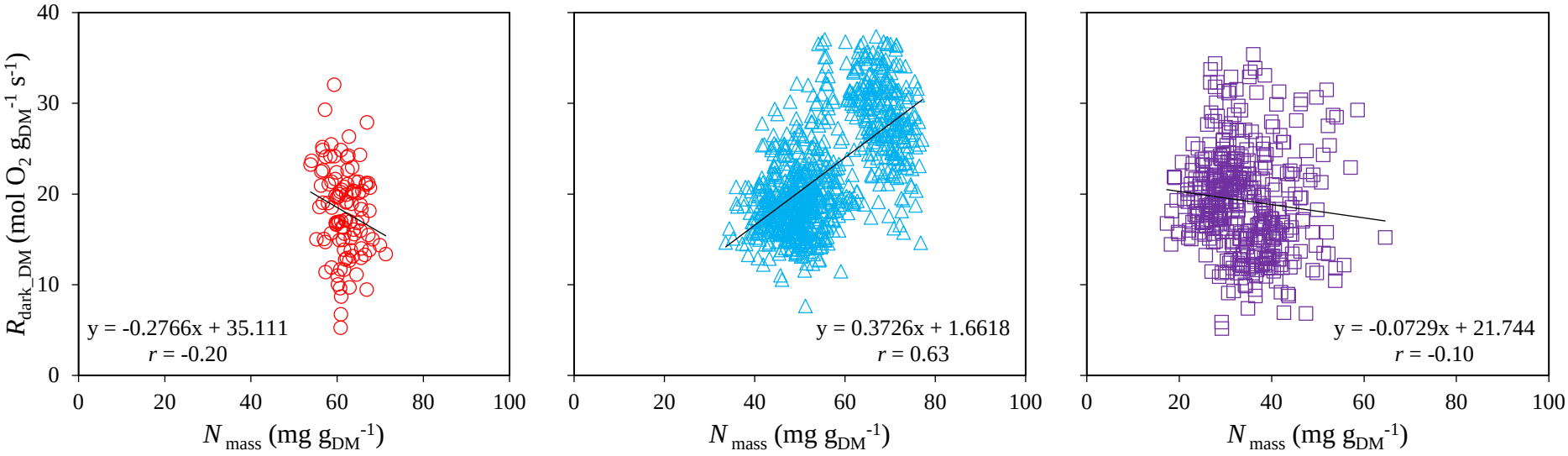

FIGURE S3 Relationships between R_{dark_LA} and **(a-c)** leaf nitrogen per square metre of leaf area (N_{area}), **(d-f)** leaf mass per area (LMA), and **(g-i)** between R_{dark_DM} and leaf nitrogen per gram of leaf dry mass (N_{mass}) for Experiment 1 (left panels), Experiment 2 (middle panels) and Experiment 3 (right panels). Pearson correlation coefficients (r) for data pooled from Experiments 1, 2 and 3 were 0.16, 0.27 and 0.38, respectively for R_{dark_LA} vs N_{area}, R_{dark_LA} vs LMA, and R_{dark_DM} vs N_{mass}.

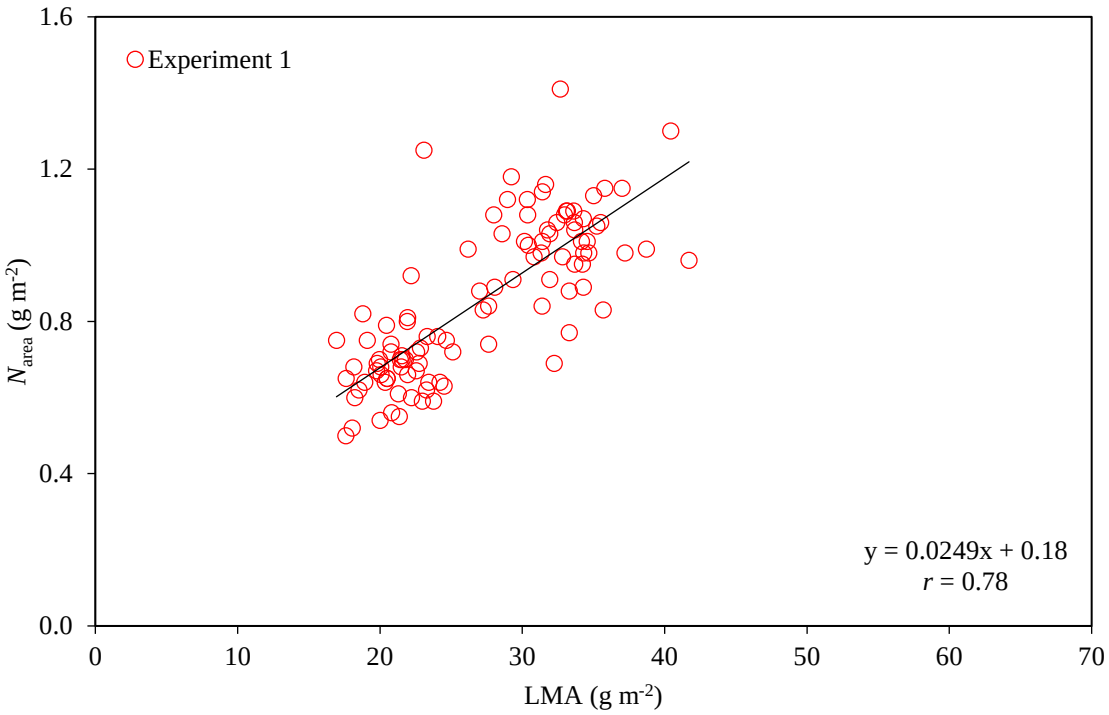
Experiment 1
y = 0.0249x + 0.18
r = 0.78
N_{area} (g m^{-2})
LMA (g m^{-2})
0.0
0.4
0.8
1.2
1.6
0
10
20
30
40
50
60
70

30

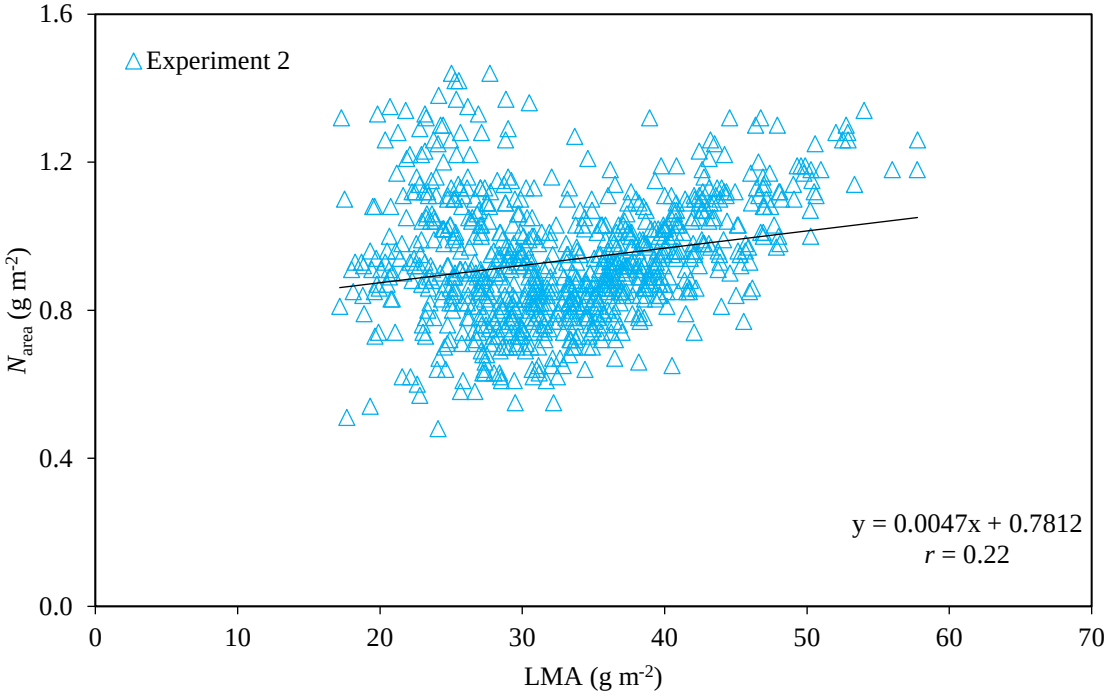
Experiment 2
y = 0.0047x + 0.7812
r = 0.22
N_{area} (g m^{-2})
LMA (g m^{-2})
0.0
0.4
0.8
1.2
1.6
0
10
20
30
40
50
60
70

31

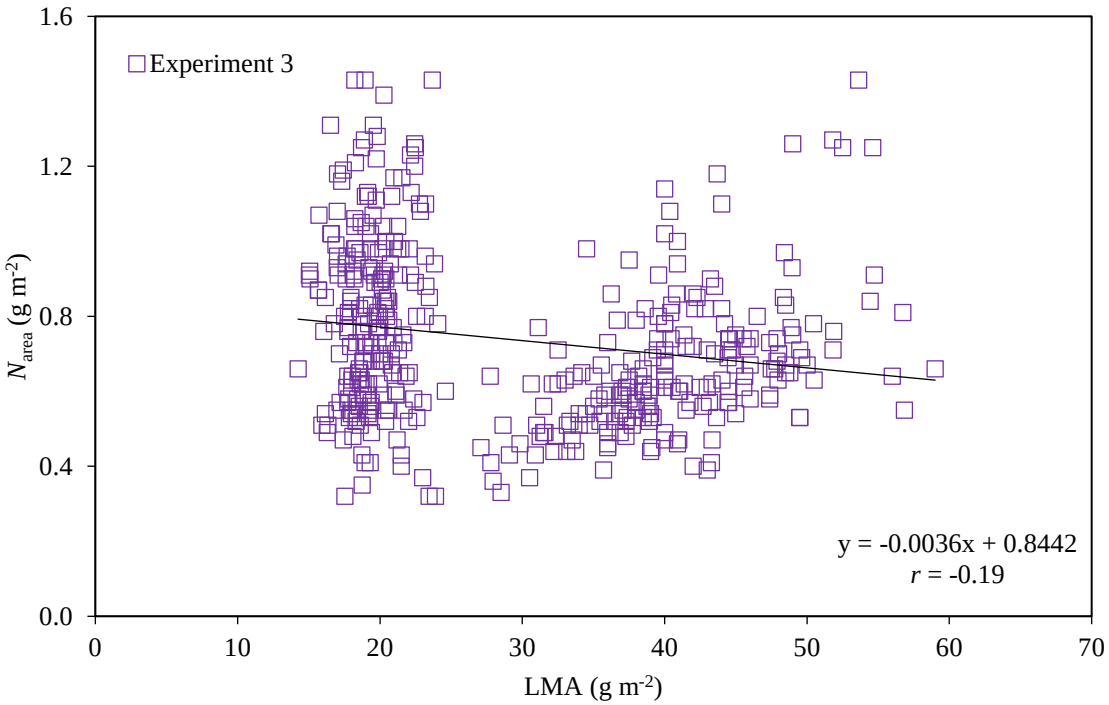

FIGURE S4 Relationship between leaf nitrogen (per square metre of leaf area, N_{area}) and leaf mass per area (LMA) for Experiment 1 **(a)**, Experiment 2 **(b)** and Experiment 3 **(c)**. For the pooled data Pearson correlation coefficients (r) was 0.12 (P<0.001).

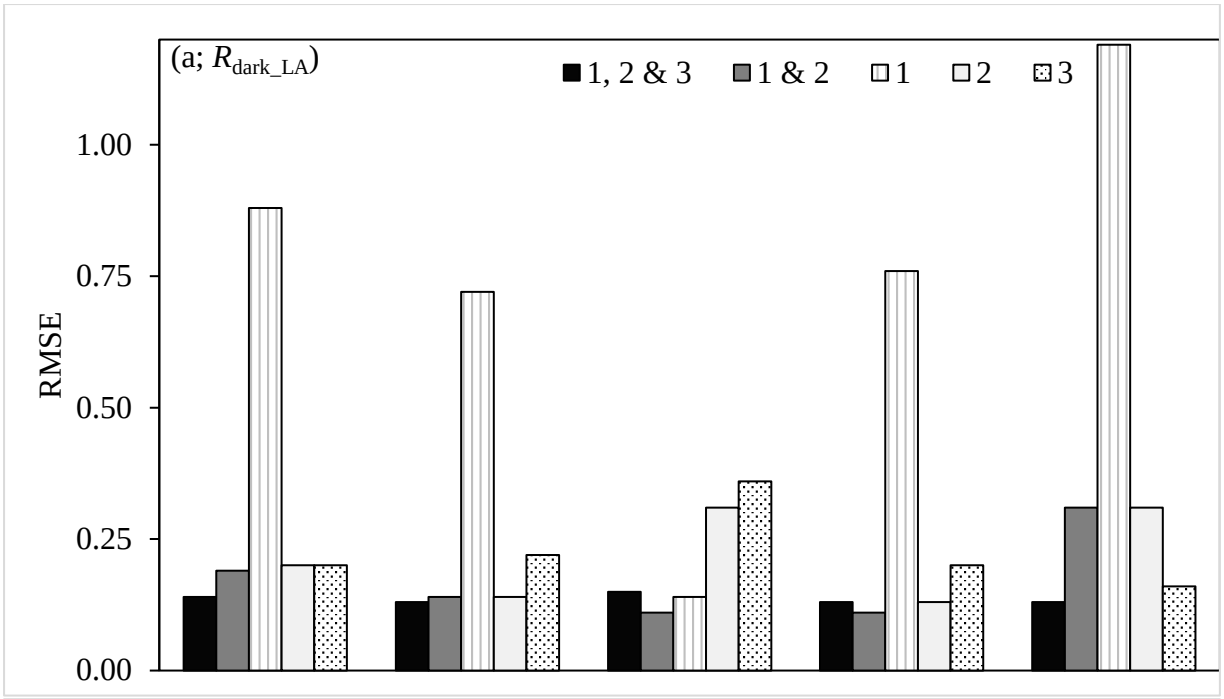
(a; R_{dark_LA})
1, 2 & 3
1 & 2
1
2
3
RMSE
1.00
0.75
0.50
0.25
0.00

36

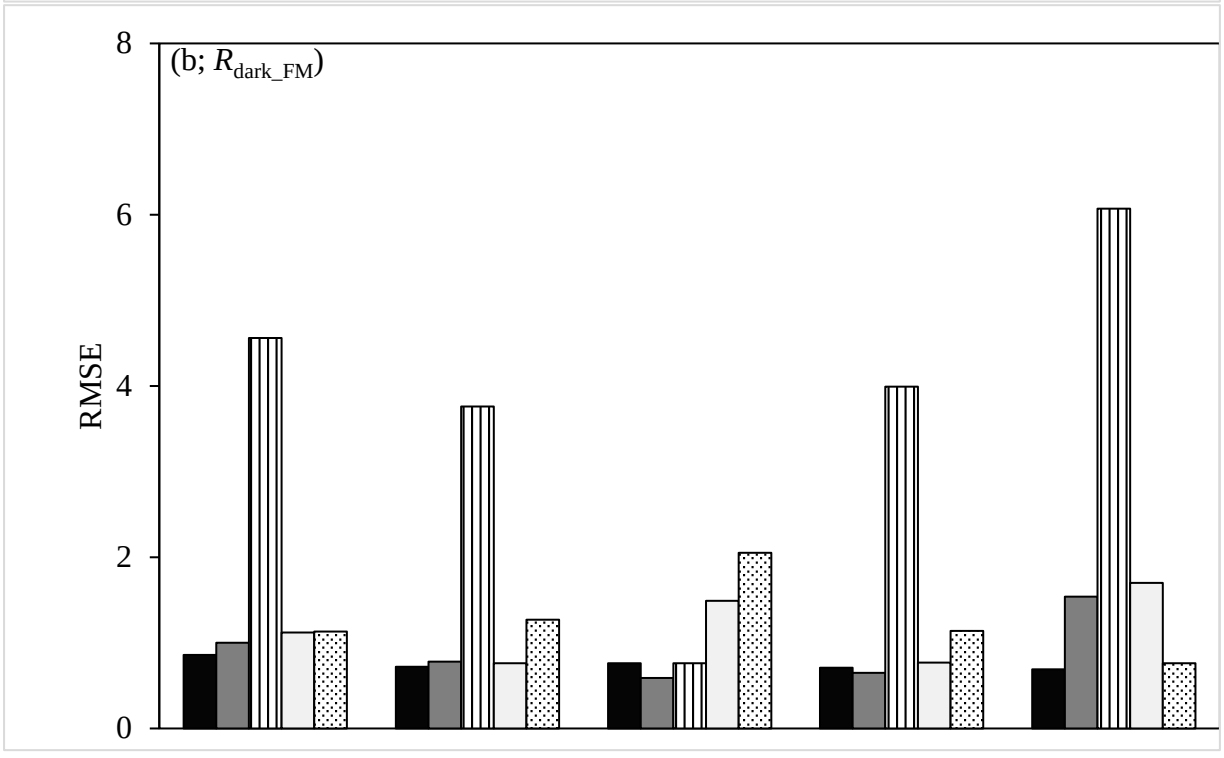
(b; R_{dark_FM})
RMSE
8
6
4
2
0

37

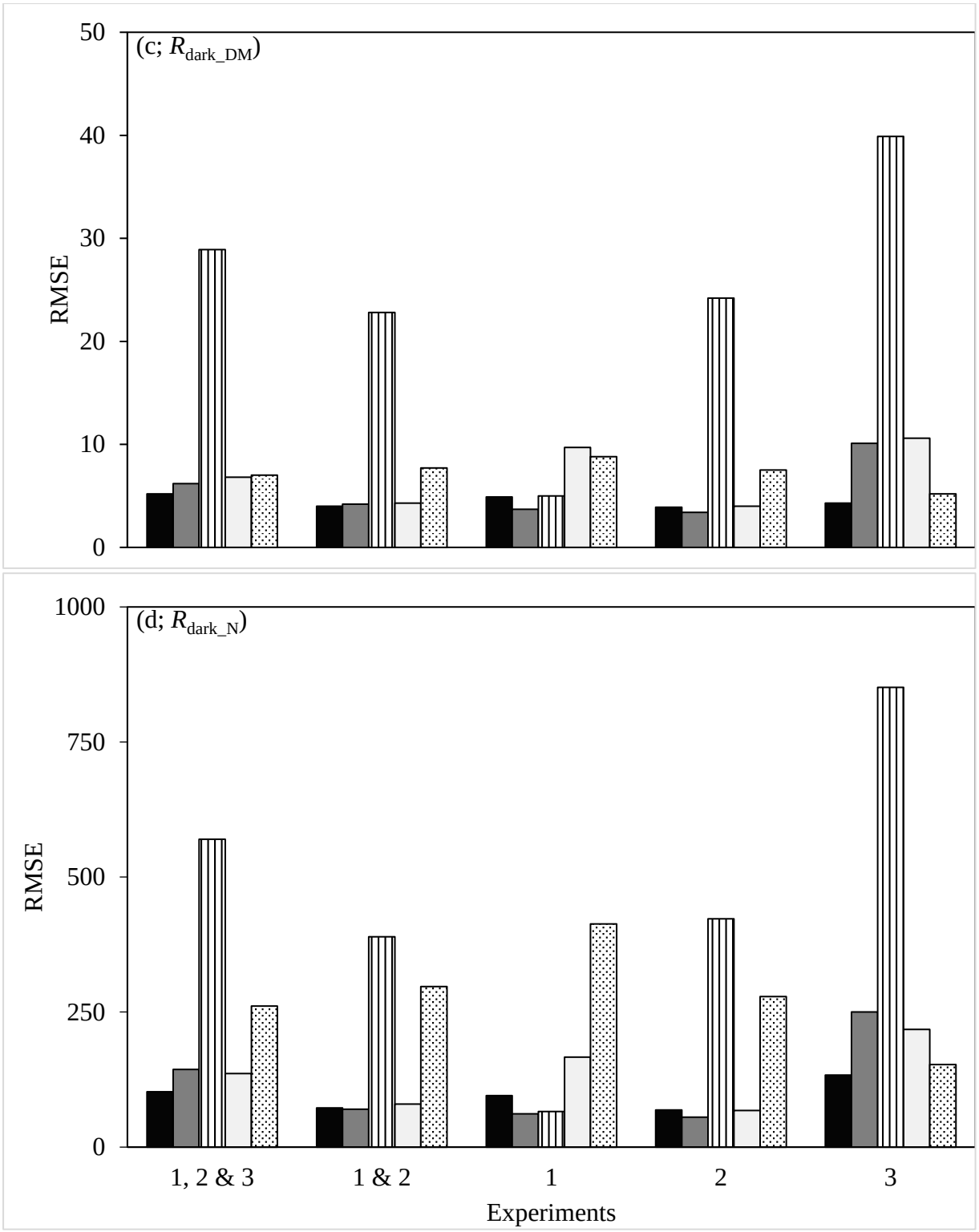

FIGURE S5 Root mean squared error (RMSE) of PLSR model used for prediction of leaf dark respiration per square metre of leaf area (R_{dark_LA}; **a**), per gram of fresh mass (R_{dark_FM}; **b**), per gram of dry mass (R_{dark_DM}; **c**), or per gram of leaf nitrogen (R_{dark_N}; **d**). PLSR models were trained on 90% of data pooled from Experiments 1, 2 and 3 (black bars) or Experiments 1 and 2 (grey bars) or from individual experiments (Experiment 1 (vertical stripped bars), Experiment 2 (white bars), or Experiment 3 (dotted bars)) and validated on the test dataset (remaining 10%).

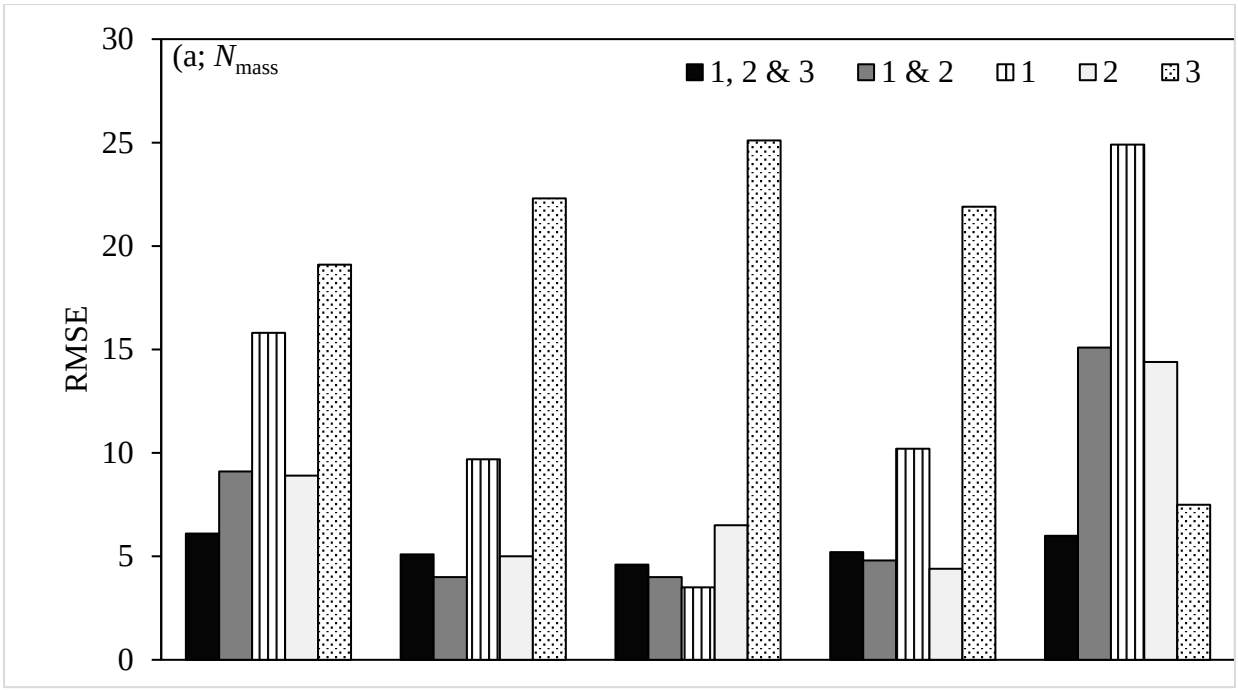
(a; N_{mass}
1, 2 & 3
1 & 2
1
2
3
RMSE
30
25
20
15
10
5
0

47

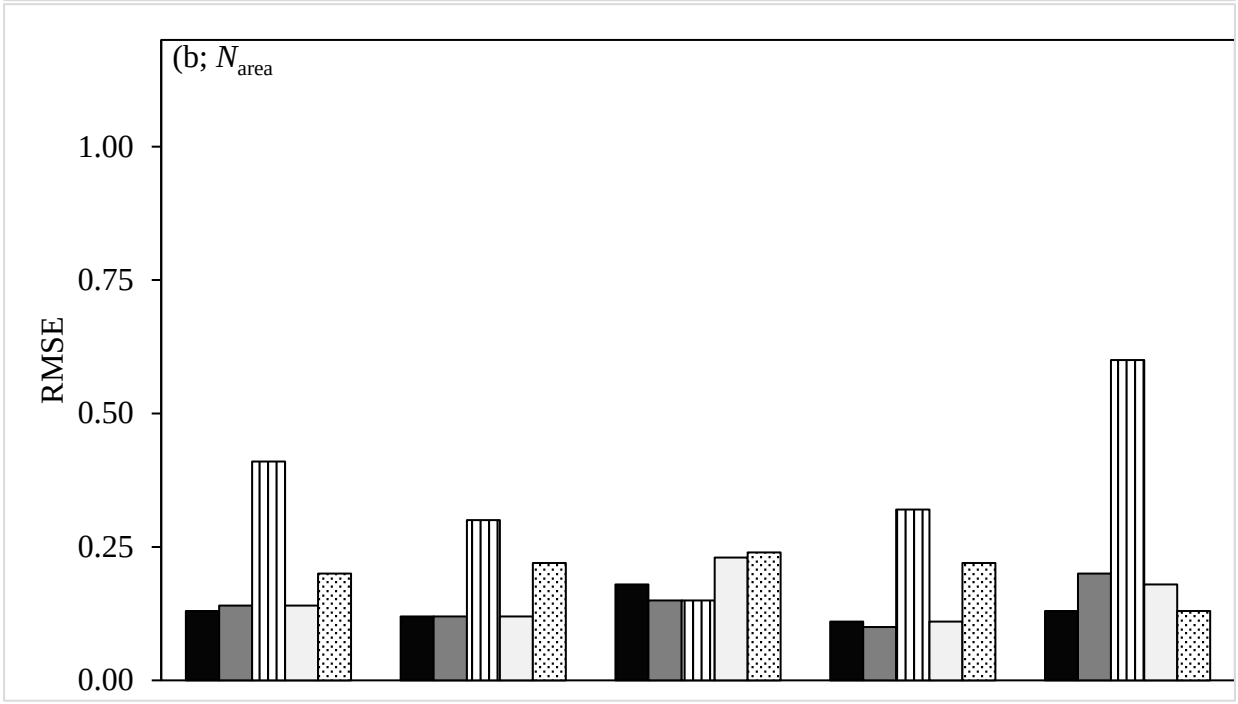
(b; N_{area}
RMSE
1.00
0.75
0.50
0.25
0.00

48

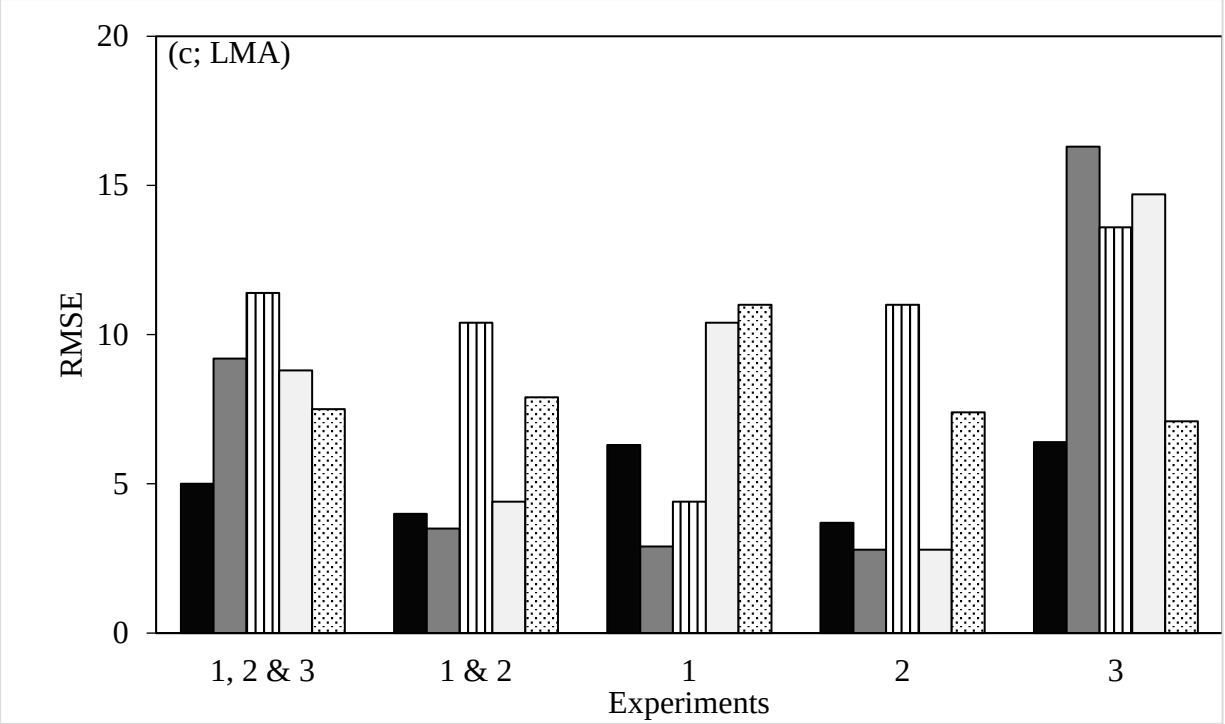

FIGURE S6 Root mean squared error (RMSE) of PLSR model used for prediction of leaf nitrogen per gram of DM (N_{mass}; **a**) or per square metre of LA (N_{area}; **b**), and LMA (**c**). PLSR models were trained on 90% of data pooled from Experiments 1, 2 and 3 (black bars) or Experiments 1 and 2 (grey bars) or from individual experiments (Experiment 1 (vertical stripped bars), Experiment 2 (white bars), or Experiment 3 (dotted bars)) and validated on the test dataset (remaining 10%).

Text S1 Multi-method ensemble

We attempted to reduce model complexity and improve model predictions by combining different regression techniques into a multi-method ensemble, an approach first suggested by Bates & Granger (1969) and shown to increase prediction accuracy (Waske & van der Linden, 2008; Du, Xia, Chanussot, & He, 2012). This is achieved by excluding bands showing low sensitivity to the response variable in all three model types (Frenich et al., 1995; Wolter, Townsend, Sturtevant, & Kingdon, 2008; Andersen & Bro, 2010). We employed the multi-method ensemble that combines PLSR, SVMR and RFR, which was recently developed by Feilhauer, Asner & Martin (2015). The ensemble identified distinct hyperspectral bands (with elevated sensitivity to the response variable) for each of the PLSR, SVMR and RFR models. These subsets of wavelengths were in turn used to model predictions of the different traits of interest and predictions compared to those developed with the full spectrum.

In the ensemble, individual model predictions of leaf R_{dark}, N_{mass}, N_{area} and LMA using either the continuous, full spectrum data or a spectral subset selected based on weightings in the multi-method ensemble developed by Feilhauer et al. (2015) were mostly similar (Table S6). Within models, differences in r^2 between full spectrum and selected subset of wavelengths were at most ±0.03 for R_{dark} and ±0.04 for other leaf traits. The use of model coefficient weighting resulted in the selection of between 173 and 271 wavelengths for R_{dark} and other leaf traits. The selected wavelengths were spread across the whole spectrum of interest. Across models the RFR performed less well in some instances (e.g. R_{dark_LA}, R_{dark_FM} and LMA) compared to PLSR and SVRM (Table S6). We found that the PLSR model exhibited better performance relative to RFR but similar performance to the SVMR model.

Citations

Andersen C.M. & Bro R. (2010) Variable selection in regression – a tutorial. *Journal of Chemometrics* 24, 728–737.

Bates J.M. & Granger C.W.J. (1969) The combination of forecasts. *Journal of the Operational Research Society* 20, 451–468.

Du P., Xia J., Chanussot J. & He X. (2012) Hyperspectral remote sensing image classification based on the integration of support vector machine and random forest. In *Proceedings of the 2012 IEEE International Geoscience and Remote Sensing Symposium (IGARSS)*, Munich, pp 174–177.

Feilhauer H., Asner G.P. & Martin R.E. (2015) Multi-method ensemble selection of spectral bands related to leaf biochemistry. *Remote Sensing of Environment* 164, 57–65.

Frenich A.G., Jouan-Rimbaud D., Massart D., Kuttatharmmakul S., Galera M.M. & Vidal J.M. (1995) Wavelength selection method for multicomponent spectrophotometric determinations using partial least squares. *Analyst* 120, 2787–2792.

Waske B. & van der Linden S. (2008) Classifying multilevel imagery from SAR and optical sensors by decision fusion. *IEEE Transactions on Geoscience and Remote Sensing* 46, 1457–1466.

Wolter P.T., Townsend P.A., Sturtevant B.R. & Kingdon C.C. (2008) Remote sensing of the distribution and abundance of host species for spruce budworm in Northern Minnesota and Ontario. *Remote Sensing of Environment* 112, 3971–3982.

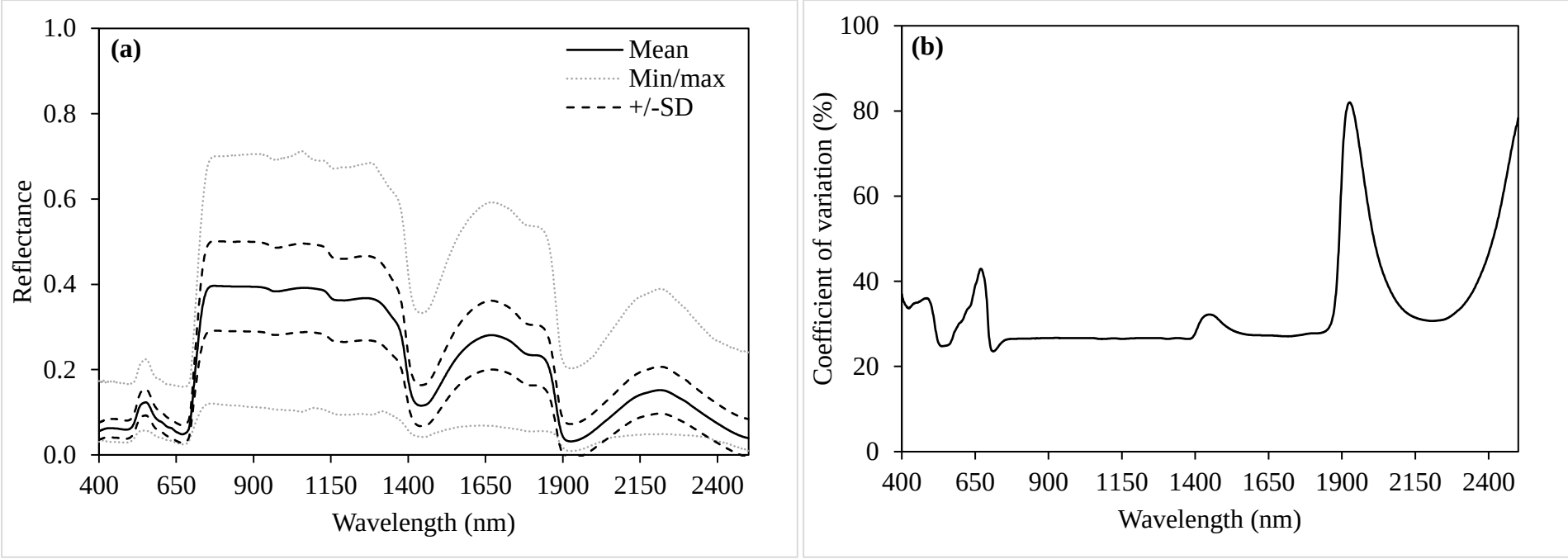

FIGURE 1 Mean (± standard deviation), minimum and maximum leaf reflectance **(a)** of wheat and spectral coefficients of variation **(b)** for three experiments (Experiments 1, 2 and 3) combined.

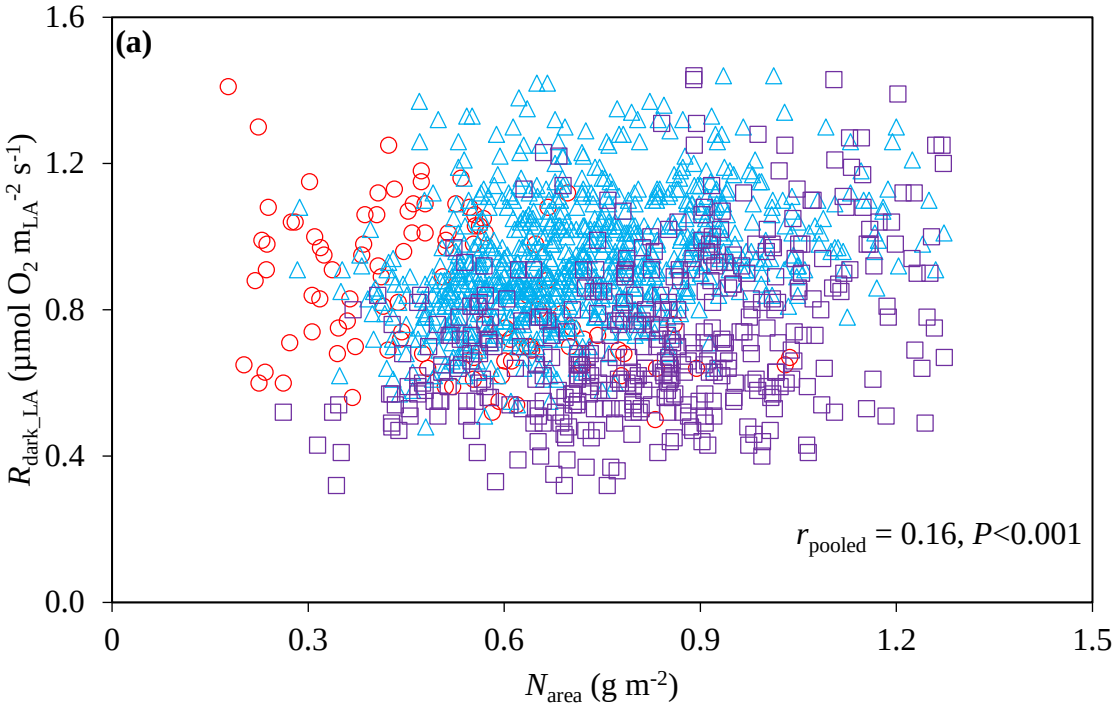
(a)
R_{dark_LA} (μmol O_2 m_{LA}^{-2} s^{-1})
1.6
1.2
0.8
0.4
0.0
0
0.3
0.6
0.9
1.2
1.5
N_{area} (g m^{-2})
r_{pooled} = 0.16, P<0.001

102

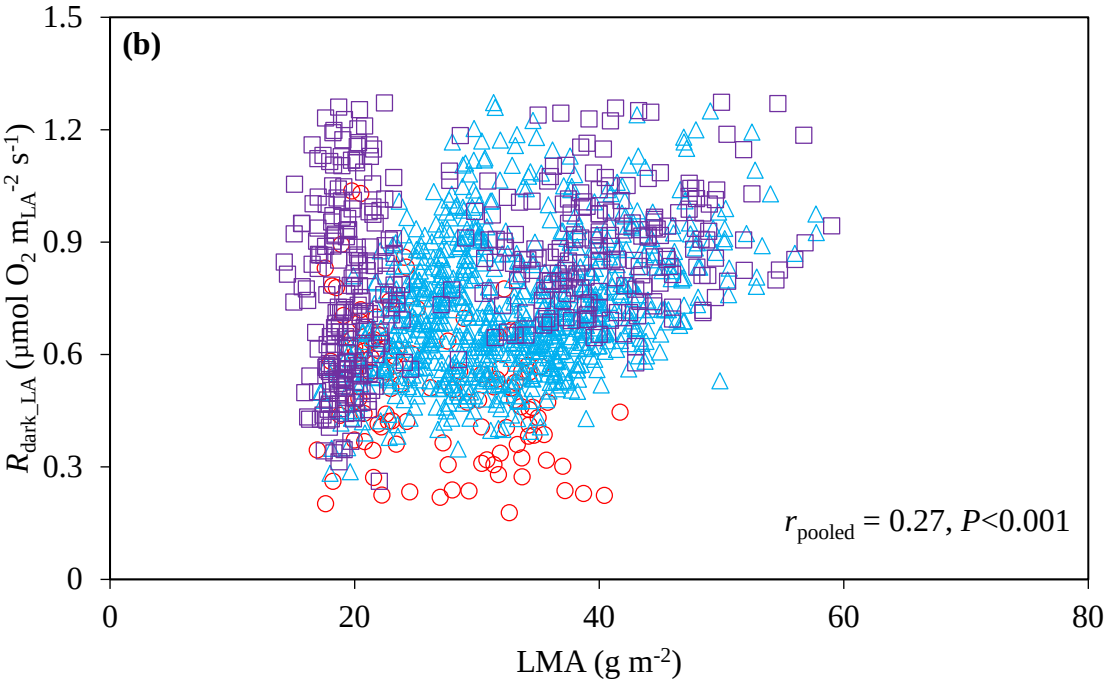
(b)
R_{dark_LA} (μmol O_2 m_{LA}^{-2} s^{-1})
1.5
1.2
0.9
0.6
0.3
0
0
20
40
60
80
LMA (g m^{-2})
r_{pooled} = 0.27, P<0.001

103

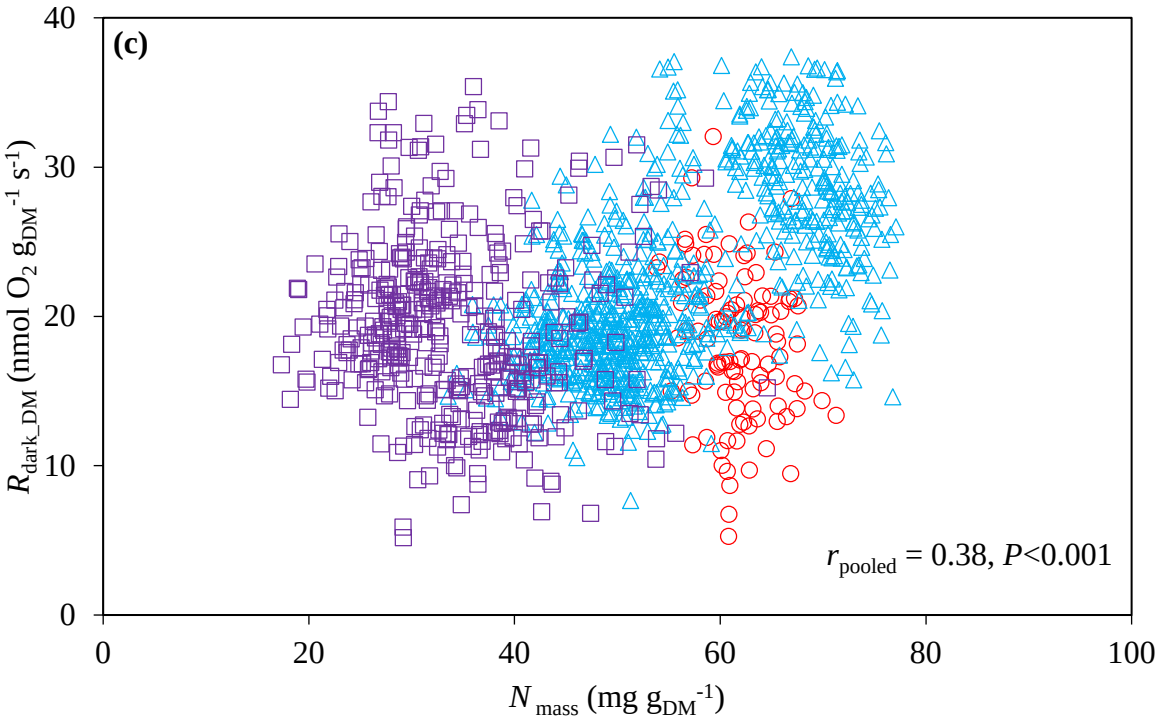

104
105 **FIGURE 2** Relationships between R_{dark_LA} and **(a)** nitrogen content per unit leaf area (N_{area}),
106 **(b)** leaf dry mass per unit leaf area (LMA), and **(c)** between R_{dark_DM} and nitrogen concentration
107 per unit leaf dry mass (N_{mass}). Pearson correlation coefficients (r) for data pooled from
108 Experiments 1, 2 and 3 are presented in the plots. For each of Experiment 1 (red circles),
109 Experiment 2 (blue triangles) and Experiment 3 (purple squares) the respective r were -0.36,
110 0.36 and 0.40 for R_{dark_LA} vs N_{area}, -0.37, 0.33 and 0.33 for R_{dark_LA} vs LMA, and -0.20, 0.63
111 and -0.10 for R_{dark_DM} vs N_{mass}.

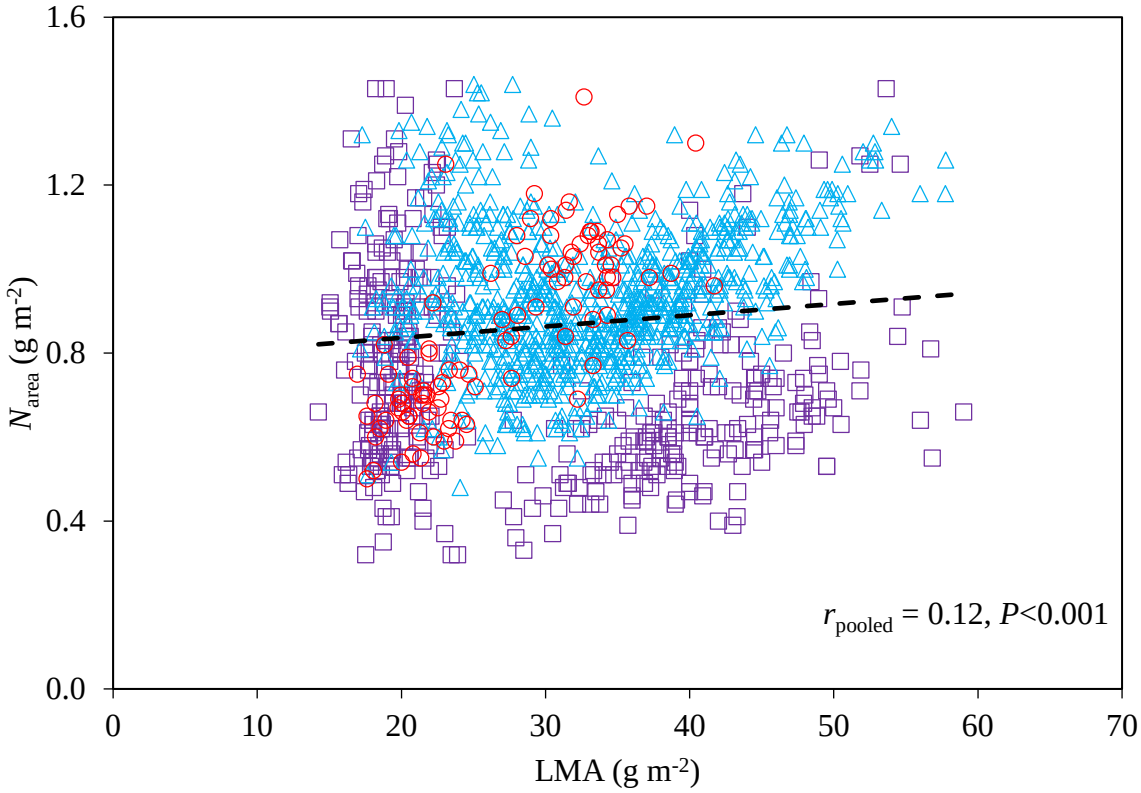

FIGURE 3 Relationship between nitrogen content per unit leaf area (N_{area}) and leaf dry mass per unit leaf area (LMA) for all three experiments combined. Pearson correlation coefficients (r) for data pooled from Experiments 1, 2 and 3 are presented in the plots. Pearson correlation coefficients (r) for each of Experiment 1 (red circles), Experiment 2 (blue triangles) and Experiment 3 (purple squares) were 0.78, 0.22 and -0.19, respectively. For all bivariate relationships between traits across all experiments, see Table 3.

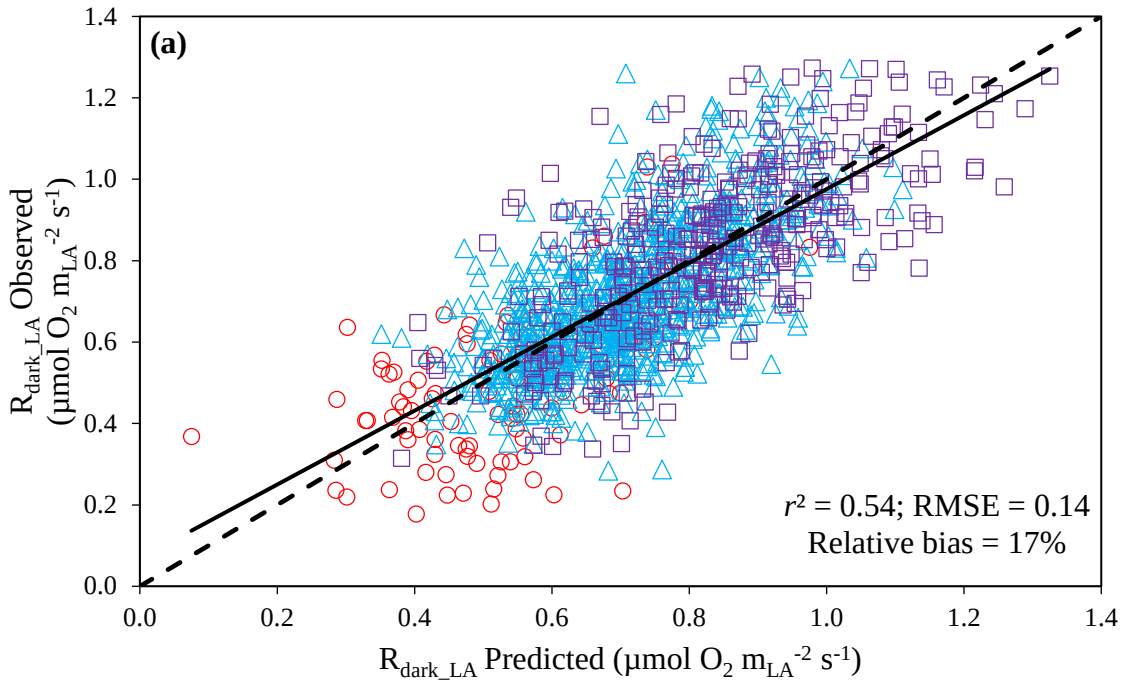
(a)
R_{dark_LA} Observed (µmol O_2 m_{LA}^{-2} s^{-1})
R_{dark_LA} Predicted (µmol O_2 m_{LA}^{-2} s^{-1})
r^2 = 0.54; RMSE = 0.14
Relative bias = 17%
0.0
0.2
0.4
0.6
0.8
1.0
1.2
1.4

119

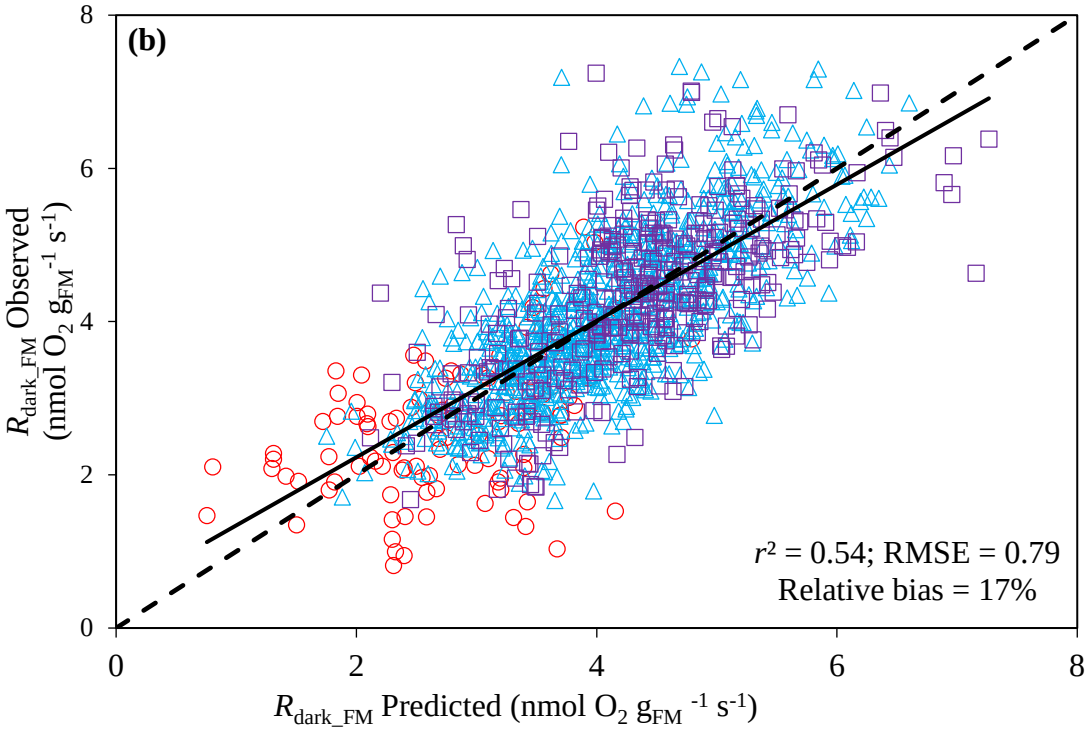
(b)
R_{dark_FM} Observed (nmol O_2 g_{FM}^{-1} s^{-1})
R_{dark_FM} Predicted (nmol O_2 g_{FM}^{-1} s^{-1})
r^2 = 0.54; RMSE = 0.79
Relative bias = 17%
0
2
4
6
8

120

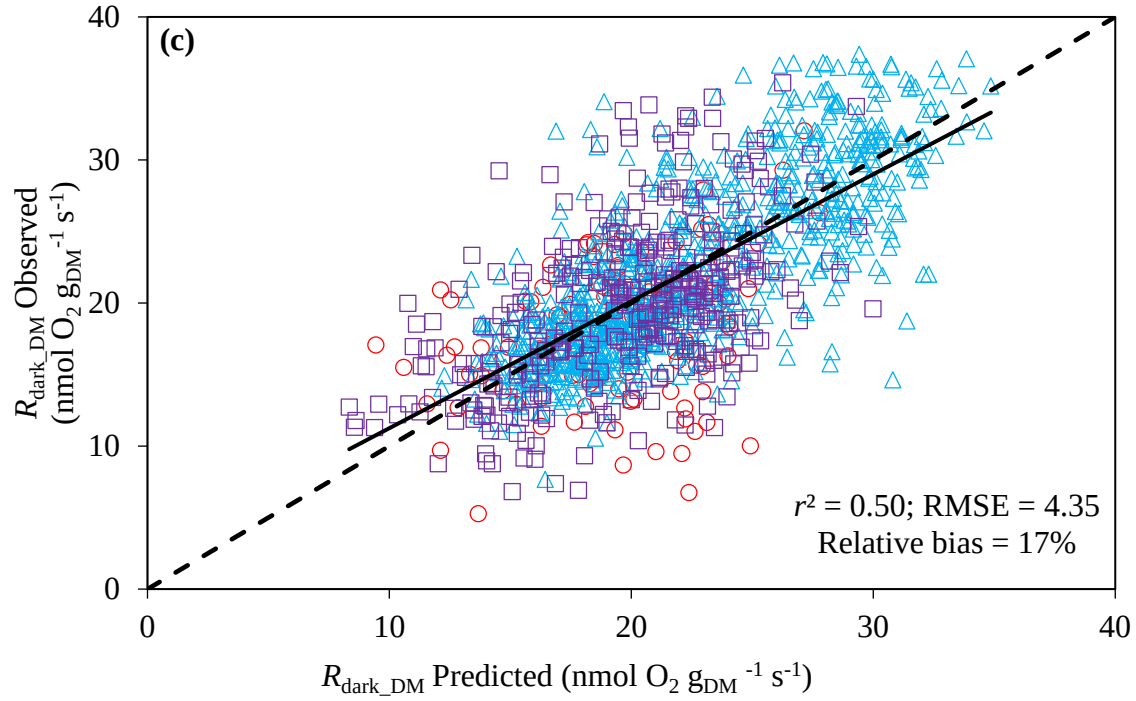

121

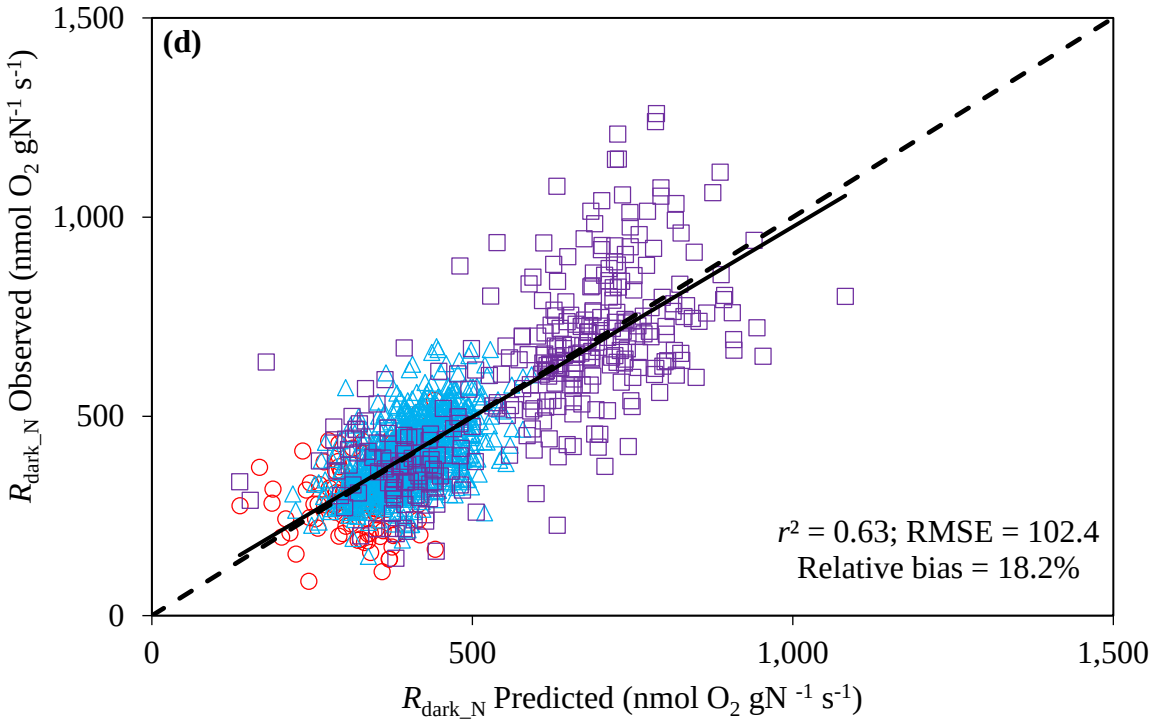

122

123 **FIGURE 4** Validation of PLSR model prediction for R_{dark_LA} **(a)**, R_{dark_FM} **(b)**, R_{dark_DM} **(c)**
124 and R_{dark_N} **(d)** using 10% of pooled data from Experiment 1 (red circles), Experiment 2 (blue
125 triangles) and Experiment 3 (purple squares) that were not used in developing the model.

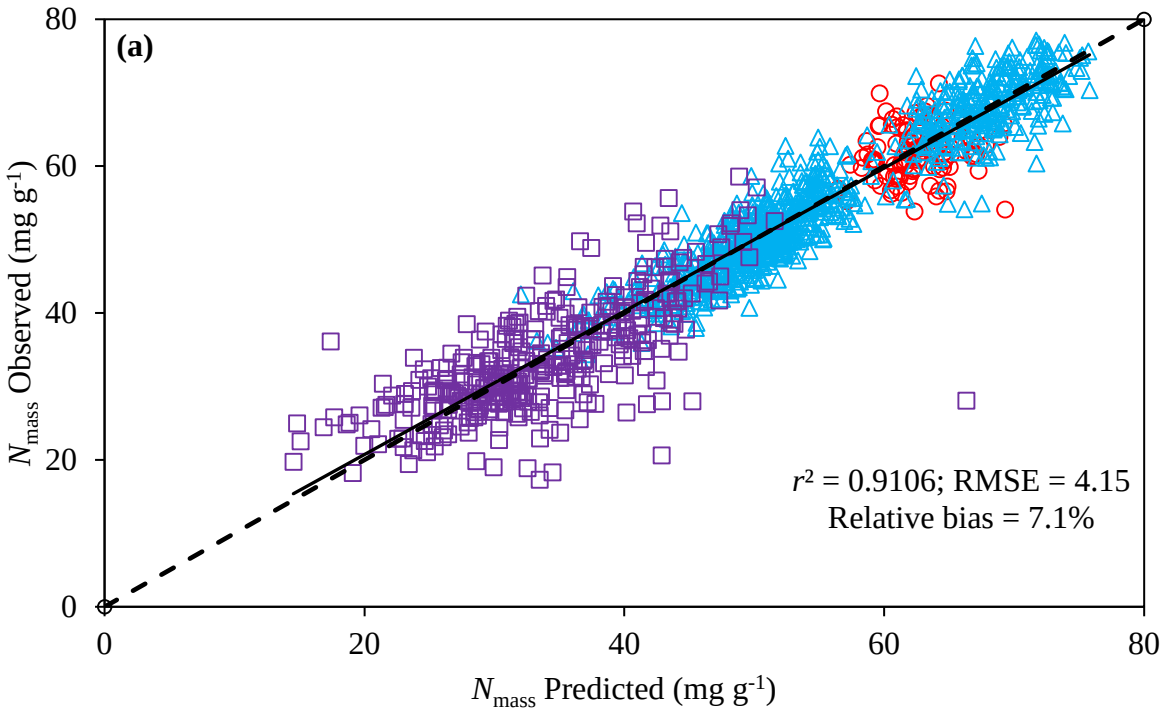
(a)
N_{mass} Observed (mg g^{-1})
N_{mass} Predicted (mg g^{-1})
r^2 = 0.9106; RMSE = 4.15
Relative bias = 7.1%
0
20
40
60
80

126

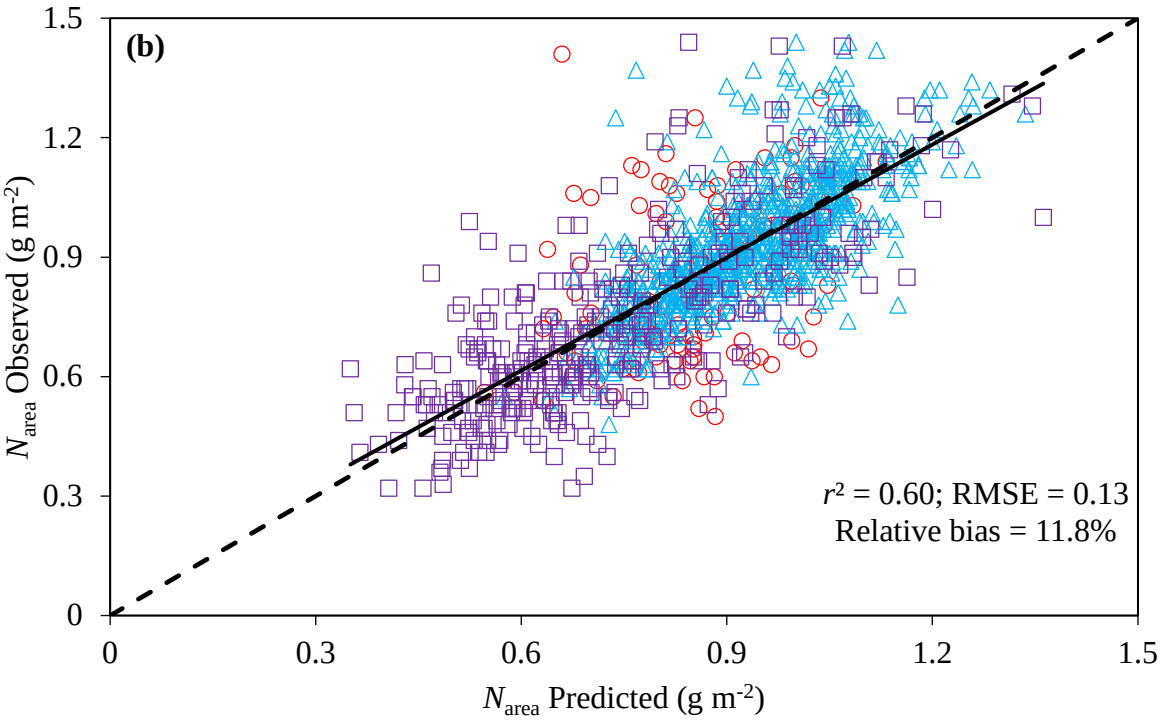
(b)
N_{area} Observed (g m^{-2})
N_{area} Predicted (g m^{-2})
r^2 = 0.60; RMSE = 0.13
Relative bias = 11.8%
0
0.3
0.6
0.9
1.2
1.5

127

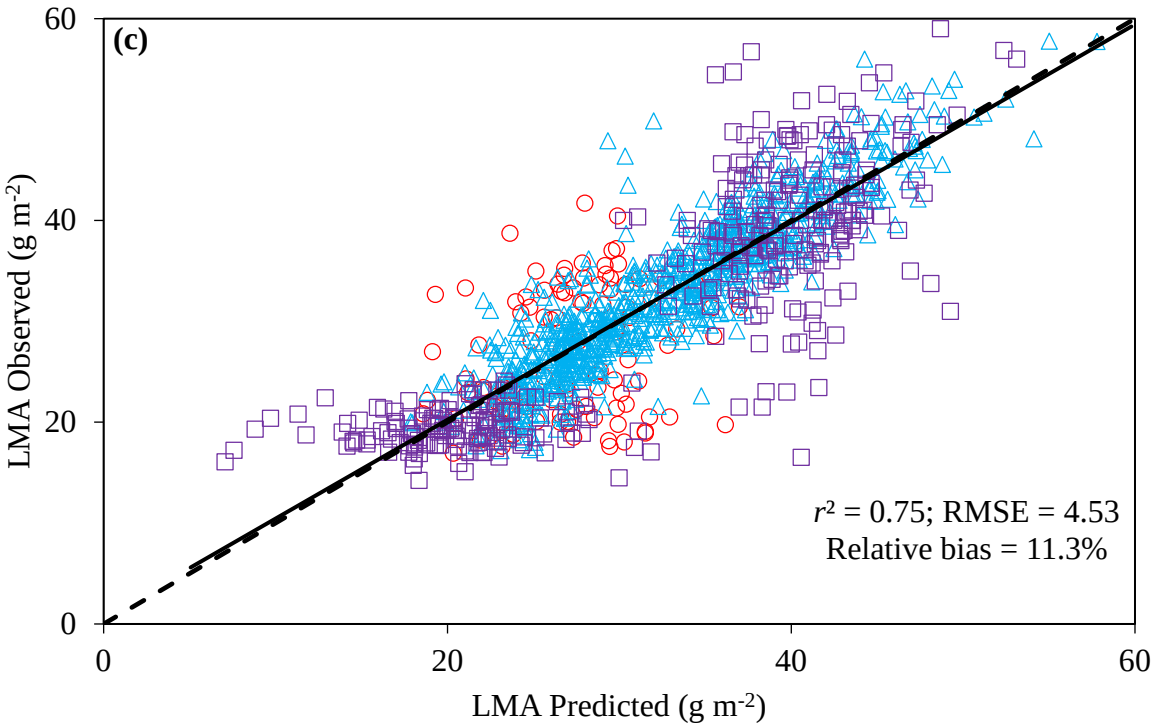

FIGURE 5 Validation of PLSR model prediction for nitrogen concentration per unit leaf dry mass (N_{mass}; **a**), nitrogen content per unit leaf area (N_{area}; **b**) and leaf dry mass per unit area (LMA; **c**), using 10% of pooled data from Experiment 1 (red circles), Experiment 2 (blue triangles) and Experiment 3 (purple squares) that were not used in developing the model.

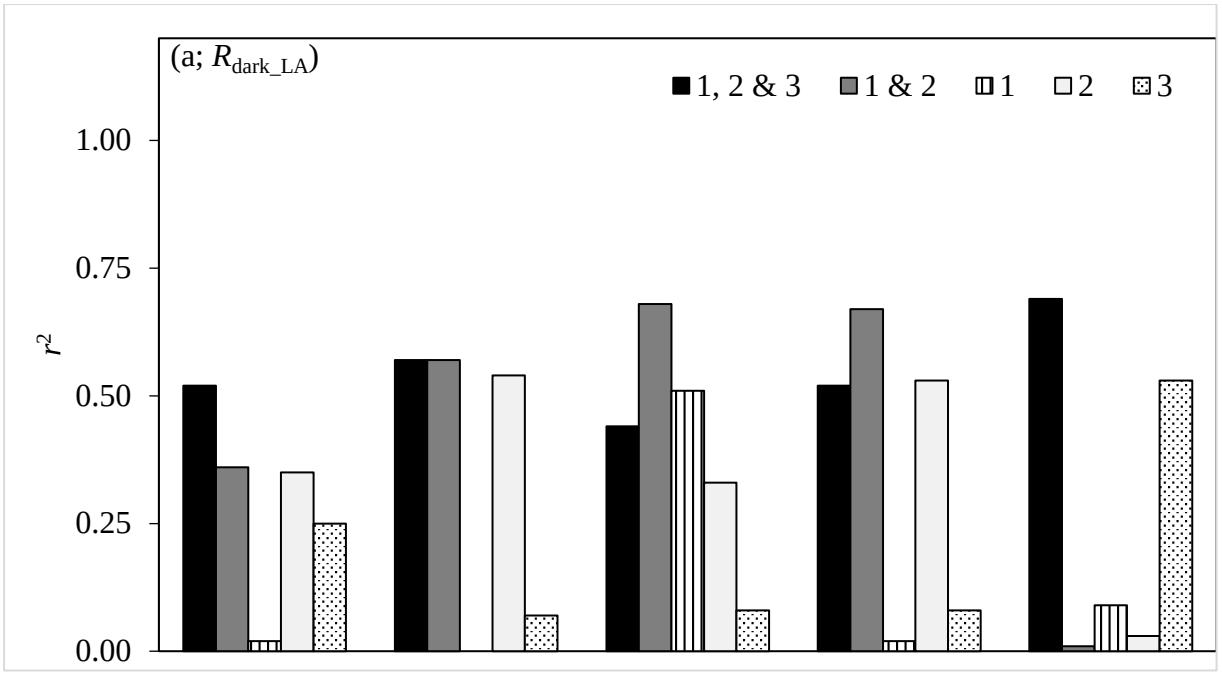
(a; R_{dark_LA})
1, 2 & 3
1 & 2
1
2
3
1.00
0.75
0.50
0.25
0.00
r^2

133

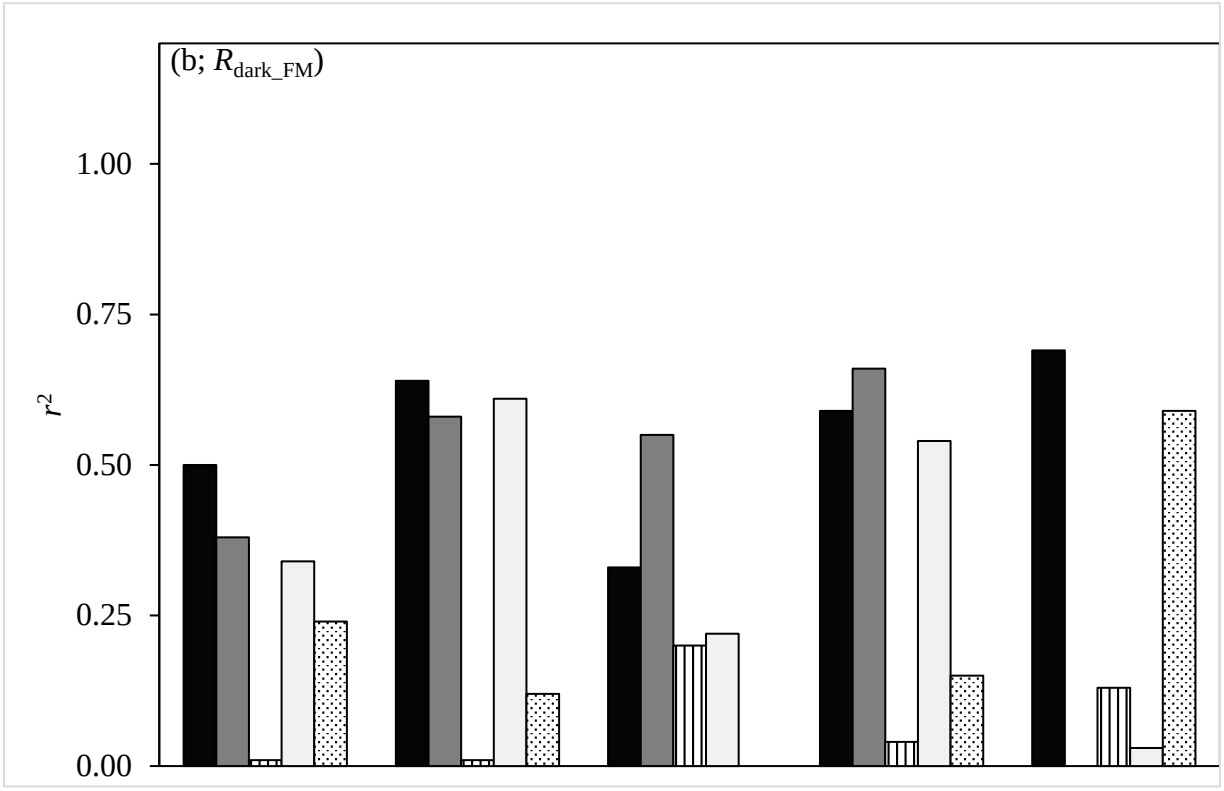
(b; R_{dark_FM})
1.00
0.75
0.50
0.25
0.00
r^2

134

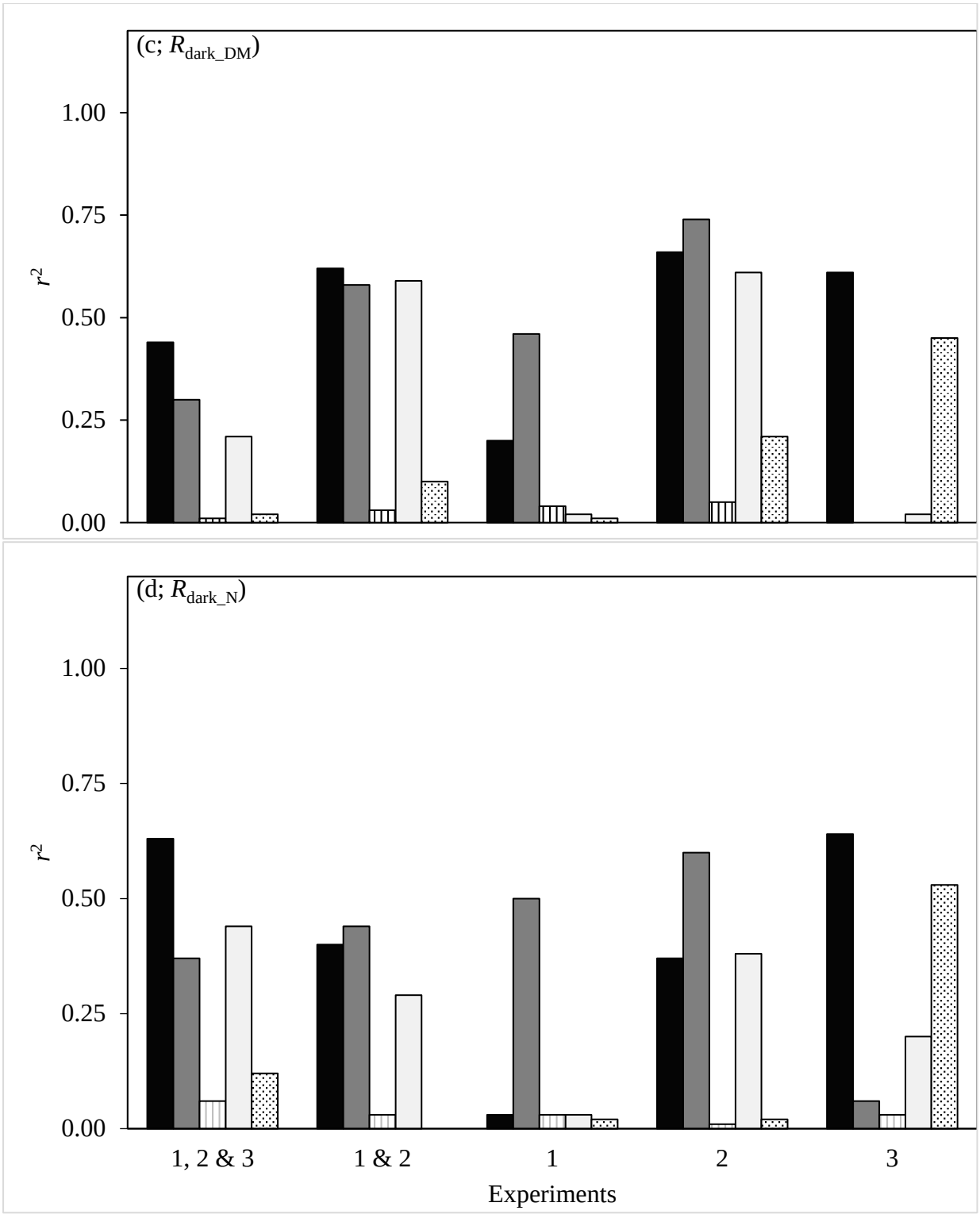

FIGURE 6 Coefficient of determination (r^2) of PLSR model used for prediction of leaf dark respiration expressed per square metre of leaf area (R_{dark_LA}; **a**), per gram of fresh mass (R_{dark_FM}; **b**), per gram of dry mass (R_{dark_DM}; **c**), or per gram of leaf nitrogen (R_{dark_N}; **d**). PLSR models were trained on 90% of data pooled from Experiments 1, 2 and 3 (black bars) or Experiments 1 and 2 (grey bars) or from individual experiments (Experiment 1 (vertical stripped bars), Experiment 2 (white bars), or Experiment 3 (dotted bars)) and validated on the test dataset (remaining 10%). See Fig S5 for root mean squared error of PLSR models for predictions of same traits.

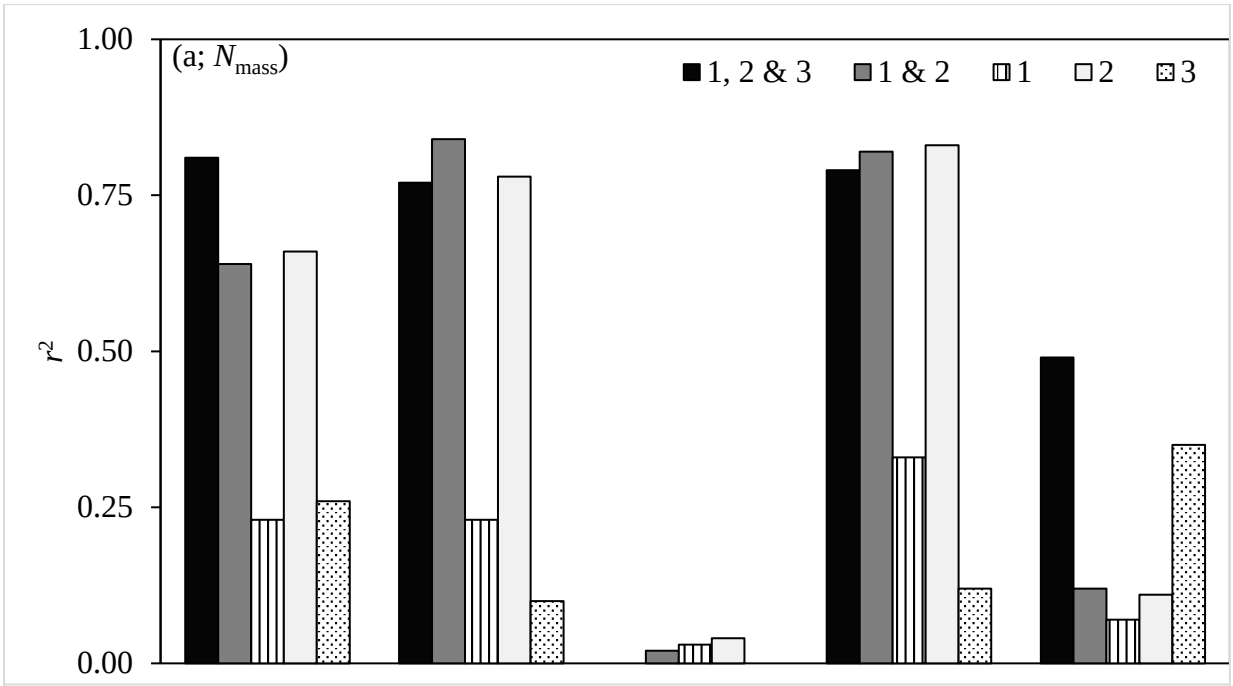
(a; N_{mass})
1, 2 & 3
1 & 2
1
2
3
1.00
0.75
0.50
0.25
0.00
r^2

145

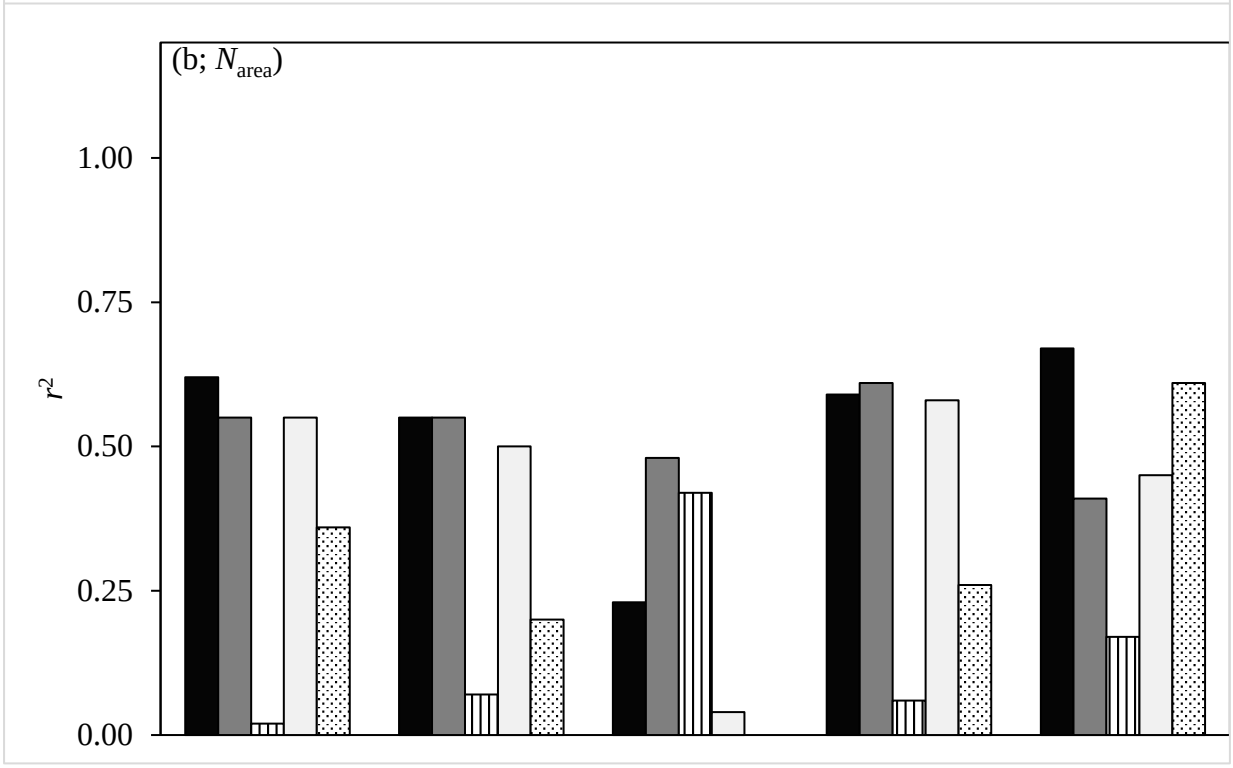
(b; N_{area})
1.00
0.75
0.50
0.25
0.00
r^2

146

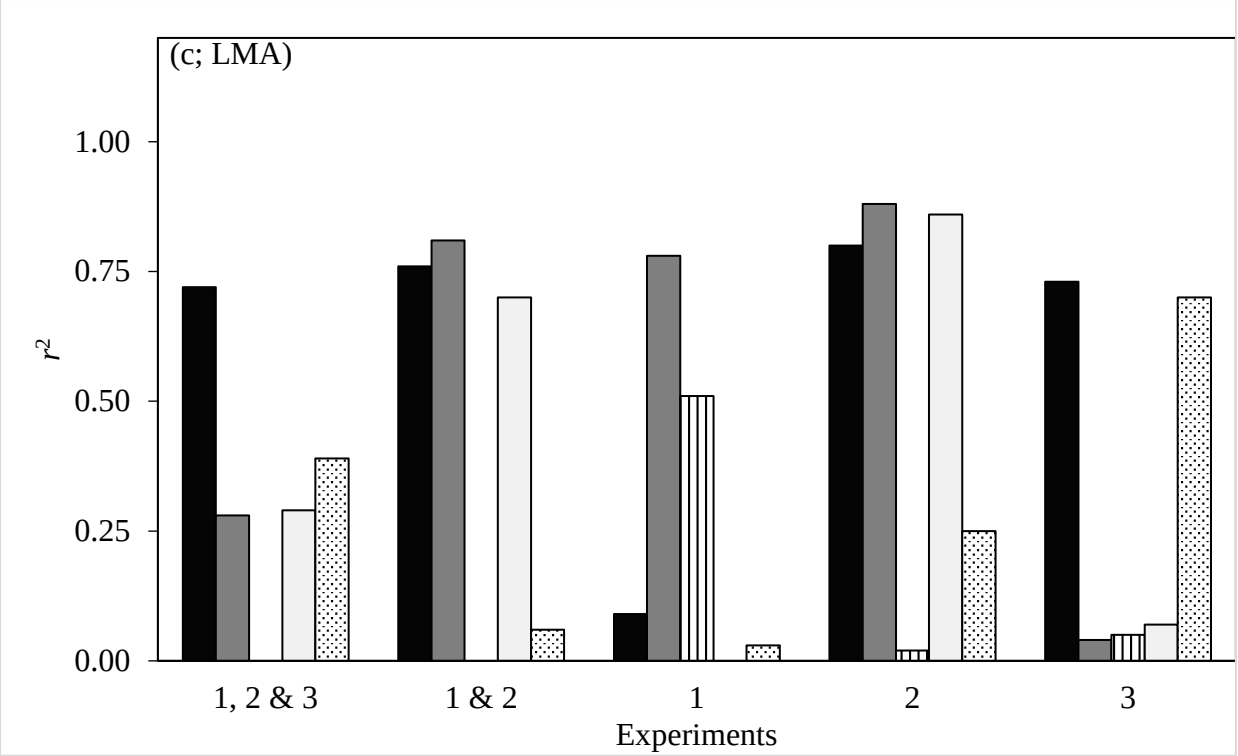

FIGURE 7 Coefficient of determination (r^2) of PLSR model used for prediction of leaf nitrogen expressed per gram of DM (N_{mass}; **a**) or per square metre of LA (N_{area}; **b**), and LMA (**c**). PLSR models were trained on 90% of data pooled from Experiments 1, 2 and 3 (black bars) or Experiments 1 and 2 (grey bars) or from individual experiments (Experiment 1 (vertical stripped bars), Experiment 2 (white bars), or Experiment 3 (dotted bars)) and validated on the test dataset (remaining 10%). See Fig S6 for root mean squared error of PLSR models for predictions of same traits.